

Review

High-power instant-synthesis technology of carbon nanomaterials and nanocomposites

Yiyang Liu^a, Zhen Ge^b, Zhongjun Li^{a,*}, Yongsheng Chen^{b,*}

^a College of Chemistry, Zhengzhou University, Zhengzhou 450001, China

^b The Centre of Nanoscale Science and Technology and Key Laboratory of Functional Polymer Materials, State Key Laboratory and Institute of Elemento-Organic Chemistry, College of Chemistry, Nankai University, Tianjin 300071, China



ARTICLE INFO

Keywords:

Carbon nanomaterials
Joule heating
Microwave plasma
Instant synthesis

ABSTRACT

Carbon nanomaterials and nanocomposites are playing a crucial role in modern science and technology. This review summarizes a kind of high-power technology (including detonation, pulsed-laser ablation, arc-electric, joule & induction heating, and microwave-induced plasma) that can synthesis such nanomaterials in seconds. First, the history and equipment setup of high-power instant-synthesis technology (HIT) are introduced. Thereafter, the growth mechanisms of carbon nanomaterials and nanocomposites are thoroughly discussed, followed by the recent developments of HIT-synthesized nanomaterials for catalyst, energy storage, and conversion applications. A comparison of the key apparatus of HIT is also presented to give a comprehensive understanding in synthesizing nanoparticles rapidly, controllably, inexpensively, and safely. Finally, the conclusion covers novel designs for promising applications, the feasibilities of mass-production, as well as the environmental considerations.

1. Introduction

Nanomaterials refer to small structures with at least one of the dimensions in the range of 1–100 nm. They are superior to the bulk materials due to their size-dependent properties. Down-size of the bulk into nanomaterials exposes massive crystalline surfaces that increase their chemical reactivity. Besides, the electrons of nanoparticles show quantum confinement by the potential wells, which significantly change their electrical, optical, magnetic, dielectric properties, etc. For example, the exfoliated monolayer graphene exhibits entirely different natures from graphite. Hot electrons of the polymeric graphene foam can be excited by a laser, then ejected through Auger-like pathways to propel the foam in the opposite direction [1]. As for organic photovoltaic devices, the nanoscale optical spacer can enhance photon absorption. Besides, the noble metallic nanoparticles can trigger the excitation of the localized surface plasmon resonance, which can increase the power conversion efficiency [2]. Attracted by the intriguing properties of nanomaterials, many efforts have been put in the control of their size & morphologies and extensive applications in the last few decades [3–30].

Nanoparticles can be either bottom-up synthesized from molecules/atoms or top-down broke from macroscopic materials via a variety of techniques that differ from their reaction media such as liquid-phase and

solid-gaseous-phase. Generally, the liquid-phase methods consist of coprecipitation [31,32], sol-gel [33], self-assembly [34], microemulsion [35], sonochemical [36], template synthesis [37], solvo-microwave [38], solvo-exfoliation [39], hydrothermal [40], electrodeposition [41], etc. The liquid-phase methods require a solvent to dissolve or disperse the precursors, then drive the reaction to form desired nanoparticles chemically by applying ultrasound, microwave, heat & pressure, mild electric current, etc. They usually require long reaction times and multi-step processing which takes tens of hours.

Besides the liquid-phase, the solid-gaseous-phase synthesis utilizes energized ion beam, laser, electric current, etc. to boost the reaction in solid or gaseous media, such as chemical vapor deposition (CVD) [42], mechanical exfoliation [43], magnetron evaporation [44], ion-beam sputtering [45], etc. They can charge the precursor with high energy (ion beam with 1000 eV [46] or current at 680 A [47]). Furthermore, they are capable of flash-synthesizing nanomaterials with high formation temperatures such as nano-sized alloy [48], heterostructure [49], and carbonaceous composite [50,51]. Among them, CVD is a delicate method to grow graphene [52], carbon nanotube [53], etc. The gaseous reactants were introduced with a suitable substrate at relatively high temperatures (600–2300 °C), then the products were layer-by-layer deposited [54,55]. Mechanical exfoliation is a simple method to

* Corresponding authors.

E-mail addresses: lizhongjun@zzu.edu.cn (Z. Li), yschen99@nankai.edu.cn (Y. Chen).

<https://doi.org/10.1016/j.nanoen.2020.105500>

Received 5 September 2020; Received in revised form 30 September 2020; Accepted 12 October 2020

Available online 20 October 2020

2211-2855/© 2020 Elsevier Ltd. All rights reserved.

separate adjacent graphene layers against Van der Waals attraction. One of the most famous demonstrations is done by Geim and his colleagues [5] who acquire single-layer graphene with a scotch-tape peeling technology. Magnetron evaporation and ion-beam sputtering are the main techniques of physical vapor deposition (PVD), in which the source materials are energized into vapor or plasma, then deposited on a substrate in a vacuum chamber with controlled thickness. In principle, PVD is solely a powerful coating method rather than synthesizing nanomaterials with morphology & composition control [56]. The above mentioned solid-gaseous-phase synthesis are occurring at a relatively high temperature compared to the liquid-phase methods. However, either they are not suitable for nanomaterials synthesis or their reaction time is long (hours to days) [57,58]. Hence they do not meet the ever-increasing demand as versatile and efficient nanomaterials synthesis technologies.

With raised recent worldwide concerns in balancing the nature and nanotechnologies, environmentally friendly manufacturing techniques are favored with the major requirements below: (i) solvent-free or use water as the solvent in purification instead of wasteful organic solvents; (ii) can produce unique nanomaterials that are difficult to produce directly using liquid-phase methods; (iii) feasible for large quantity manufacturing; (iv) one-step or few-step synthesis with reaction time in seconds (overall low energy input). Few methods meet these requirements. Under the given circumstance, a group of technologies stood out to sustain the responsibilities. We boldly categorized them as high-power instant synthesis technology (HIT).

HIT, such as detonation (DET) [59], pulsed laser ablation (PLA) [60], arc electric (AE) [61], joule & induction heating (JIH) [62,63], and microwave-induced plasma (MIP) [64], is a class of methods that applies enormous energy in a relatively short time (microseconds to several minutes) in synthesizing nanomaterials. Fundamental principles of HIT were discovered over a century ago, e.g. synthesis of trinitrotoluene (TNT), discovery of continuous electric arc [65], discovery of electric-heat phenomenon [66], and spark transmitter microwave device [67]. Yet many of HIT were only used for military purposes until the end of World War II. After that, they were applied in civil applications like mining explosives, barcode scanner, electric heater, welding, food heater, etc. The rise of HIT is on account of the discovery of carbon-nanomaterials (CNM), e.g. fullerene [3], nanodiamonds (ND) [59], carbon nanotubes (CNT) [4], graphene [5], carbon nanofibers (CNF) [68], in the applications of bioimaging, drug delivery [69], artificial tissue engineering, seawater desalination, electromagnetic-wave (EM) shielding, catalysis [70], sensor [71], pollutant degradation [72], photovoltaic cell [73], energy storage device [74] (Fig. 1). The applied high power promotes HIT ideals candidate in synthesizing nanostructures in seconds.

This review will focus on the fundamental mechanisms and promising developments of HIT. It consists: (i) a brief account on the discovery of HIT and their setups; (ii) summary of the formation mechanisms of HIT synthesized nanomaterials; (iii) signposts as to where HIT can be well developed. Peer-review papers about individual synthesis technology in specific fields have been published [75–80], yet the summative comparison of HIT has not been made. The comprehensive understanding of HIT may address most of the barriers that we believe must be overcome before they can produce nanoparticles approaching the theoretical properties. At the end of this review, insights into novel designs and promising applications of HIT will be proposed.

2. Hit for the synthesis of carbon-nanomaterials

Carbon-based nanomaterials are indispensable for the prosper of materials science such as ND [81], CNF [82], fullerene [3], multi-walled carbon nanotubes (MWCNT), single-walled carbon nanotubes (SWCNT), and graphene [5]. They possess unique electronic, optical characteristics, mechanical stability, and ease of chemical modification thus being

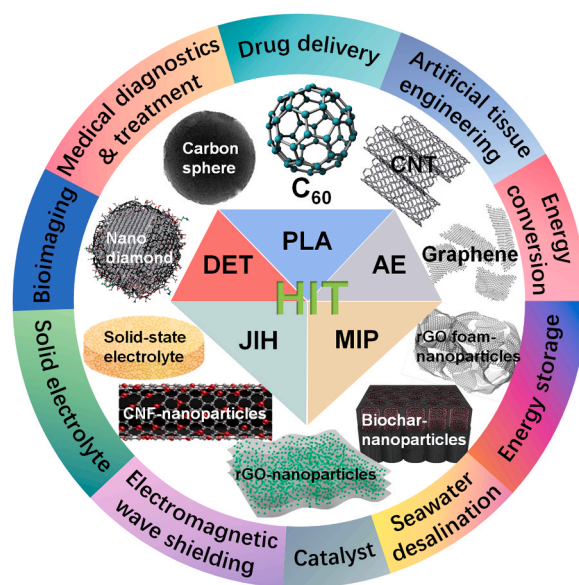


Fig. 1. Schematic overview of the topics covered in this progress review. Inset figures are reproduced with permissions.

applied in extensive fields (Fig. 2). Different from the top-down exfoliation, HIT charge the precursors with high energy, which is capable in forming sp^3 carbon bonds ($284\text{--}368\text{ kJ mol}^{-1}$ for the single σ -bond) in ND/carbon dots [83] and sp^2 carbon bonds (615 kJ mol^{-1} for the double σ and π bond) in fullerene [73], CNT [84] and graphene [85] via a bottom-up route [86]. Early HIT such as detonation, PLA, and AE, was introduced regard to the synthesis of representative CNM in this section.

2.1. Detonation

2.1.1. Discovery of detonation and setup

In the early 1960s, scientists in All-Russian Scientific Research Institute of Technical Physics discovered the detonation shock waves of TNT-hexogen mixtures may provide enough energy to compress the carbon source into nanoscale diamond particles [81]. However, it remains unrevealed as part of the nuke research due to military confidentiality until the end of the 1980s. Soon after that in the 1990s, ND has been widely applied in biomedical applications such as drug delivery [87], bioimaging [88], and tissue engineering [89] due to its less toxicity than other CNM [90]. Among all the efforts in synthesizing ND, detonation is the primary method due to high yield (15% of the weight of the explosive) [91], controllable size, and flexible for applications [92,93].

Fig. 3 shows the schematics of the detonation process. A cylindrical charge (TNT-hexogen mixture) is placed in the blast chamber. Then the blast chamber is filled with inert gas or water/ice as the dry and wet method, respectively. The charge is ignited by an electric spark remotely. Finally, the soot or suspension was collected via the receiving tank or cyclone separator.

2.1.2. ND formation mechanism of detonation and energy storage applications

Detonation is a stunning technology that synthesizes nanomaterials by a controlled explosion in a closed chamber. There are two basic requirements for detonation synthesis of ND, thermodynamic conditions (temperature and pressure) and suitable precursors. As discussed in the setup, the TNT-hexogen not only creates the high-intensity shock wave, it also provides excess carbon to form the ND (Fig. 4a) [95]. It is commonly accepted that the ND is formed by fast nucleation in a supersaturated carbon source environment [96]. However, the growth mechanism of detonation ND remains debatable due to it consists of a series of complex processes including decomposition of explosive

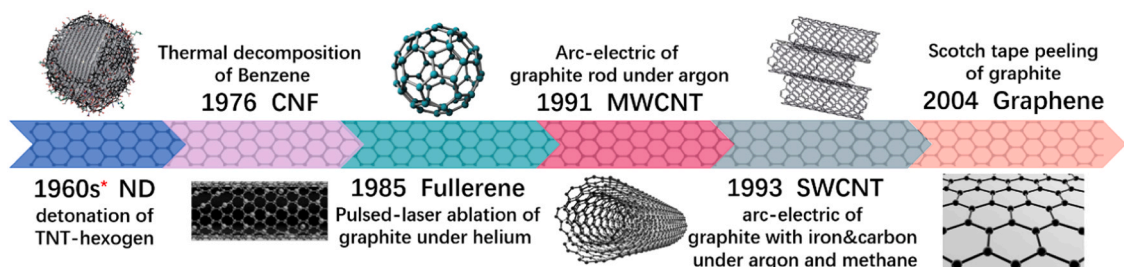


Fig. 2. Schematic overview of the discoveries of CNM: ND, CNF, fullerene, multi-walled & single-walled CNT, and graphene.

*Report of exact year is not available. Inset figures are reproduced with permissions.

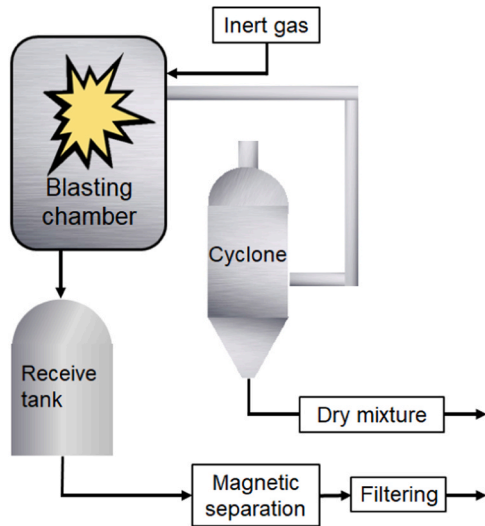


Fig. 3. Detonation synthesis of ND: flow chart of the process.

Reproduced with permission from [94].

molecules, nucleation of the core, recombination of a series of molecules & atoms, and ceases of the surface growth.

The early arguments are focused on the primary seed and carbon source. Babushkin [97] presented a mechanism that TNT-hexogen was completely decomposed into atoms during the explosion. The carbon atoms are the seeds of amorphous carbon formation, then it undergoes a phase transformation into diamond. Nonetheless, proofs were given to oppose the complete atomization theory. Danilenko [98] suggested a mainstream viewpoint of a vapor-liquid-crystal growth route based on the Jouguet-Chapman Phase diagram [99–101]. Similar standpoints were also presented that carbon atoms are condensed into nanoclusters as the seeds ($d < 1$ nm) [102] when the pressure and temperature fall along the isentrope line (Fig. 4b). Then the nanoclusters coalesce into liquid droplets in sizes of 1–2 nm as the mediates. Finally, the nanodroplets crystallized into ND (Fig. 4c). Breusov [103] made a comparison between the energy released from TNT-hexogen detonation (488.8 kcal/mol) [104] and energy from the chemical bonds of the molecules of TNT-hexogen (716 kcal/mol) [105], which indicates that the formation of free carbon atoms is unachievable. Lin [106] suggests that the emergence of cyclohexane is the starting point in the diamond formation and the collision of these carbon skeletons promotes the nuclei-mesostructure-ND formation route. On the other hand,

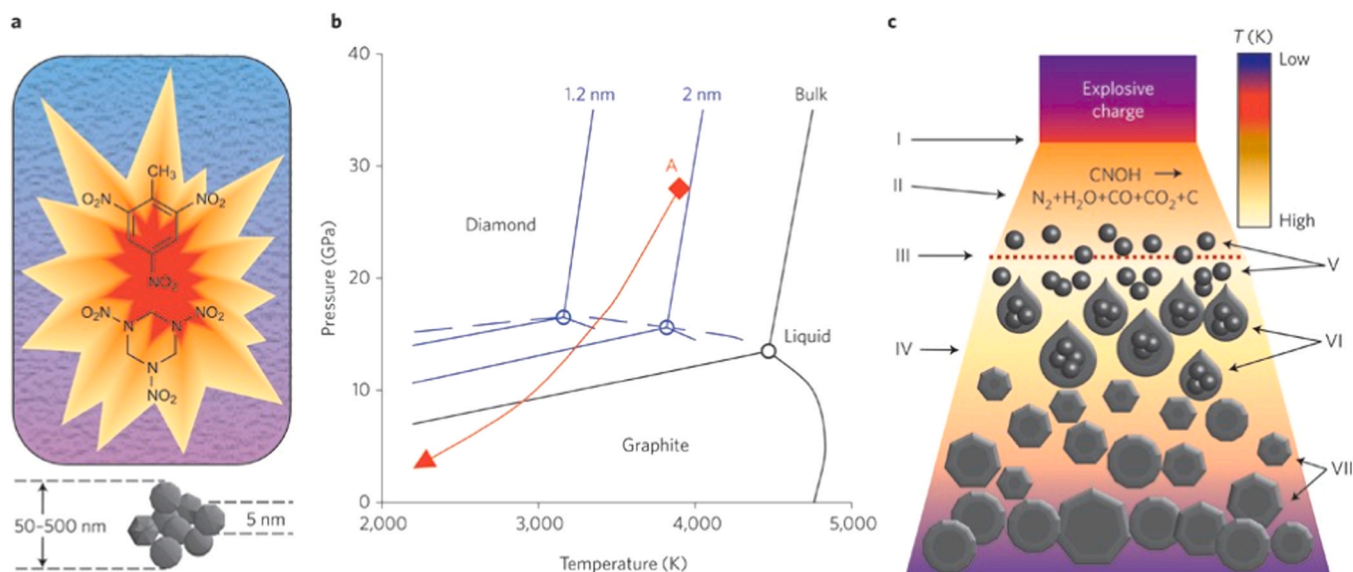


Fig. 4. (a) Explosives with a negative oxygen balance are detonated in a closed metallic chamber in an atmosphere of N_2 , CO_2 , and liquid or solid H_2O . (b) Phase diagram showing that the most stable phase of carbon is graphite at low pressures, and diamond at high pressures, with both phases melting when at temperatures above 4500 K. During detonation, the pressure and temperature rise instantaneously, reaching the Jouguet point (point A). (c) Schematic of the detonation wave propagation showing (I) the front of the shock wave caused by the explosion; (II) the zone of chemical reaction in which the explosive molecules decompose; (III) the Chapman–Jouguet plane (where P and T correspond to point A in Fig. 4b, indicating the conditions when reaction and energy release are essentially complete); (IV) the expanding detonation products; (V) the formation of carbon nanoclusters; (VI) the coagulation into liquid nanodroplets; and (VII) the crystallization, growth, and agglomeration of nanodiamonds.

Copyright 2018, Springer. Reproduced with permission from [59].

Anisichkin [107] performed an isotope study that shows the majority of ND is produced from the TNT instead of hexogen, which further refutes the theory that the molecules are all decomposed to carbon atoms.

Opinions differ in the size control, the role of hydrogen, and phase transformation & graphitization as well. Titov [108] reported that the size of detonation ND does not increase with the growth conditions based on an experiment of varying charge mass from 0.1 to 1.0 kg. Yet Danilenko [98] evidenced that the size of ND grows from 4 to 6 nm when the charge weight increased from 0.6 to 10 kg, and it can reach an average size of 8 nm in a 140 kg detonation [109]. He also indicated that the carbon black is from amorphization, thus no ND graphitization occurs during the expansion. It is against the theory that the carbon loss from diamond to carbon black is due to graphitization [110]. Tolochko [111] inferred that the growth mechanism of detonation ND is similar to CVD in which the hydrogen plays an important role in preventing graphitization and facilitating the ND growth from methyl radical. He claimed it is a chemical process from Alkyls and free radical C_xH_y to ND rather than the phase transformation. However, Dolmatov [112] proposed that the ND growth is irrespective of the use of hydrogen-based charge (TNT, hexogen) or a hydrogen-free charge (benzotrifuroxane). He drew a theory based on systematic calculations of the bonding energy in which the radical-like adamantane are the seeds, and dimer C_2 is the main building units for ND growth.

Through the growth mechanism of detonation ND remains controversial, ND have drawn huge attention in energy storage applications. The high specific surface area of ND guarantees a good supercapacitive performance based on previous work [113]. Portet [114] annealed ND in vacuum at temperatures from 1170 to 2170 K, which exhibits specific capacitances of 70–100 $F g^{-1}$. Facial surface modification of ND doped with boron [115], nitrogen [116], and phosphorus [117] can alter the electronic structure of ND, which could further facilitate their applications in catalysts or supercapacitors. Yu [117] report a phosphorus-doped ND with good capacitive performance up to 63.56 $mF cm^{-2}$ at the scan rates of 20 $mV s^{-1}$. Besides, ND can exhibit improved specific capacitance when incorporated with electrochemically active polymers. Kovalenko [118] reported a polyaniline-ND composite with specific capacitance of 640 $F g^{-1}$ and up to 10,000 charge-discharge cycles. Furthermore, ND can be incorporated with CNT [119], rGO [120], and redox-active materials such as ruthenium oxides [121] for highly improved electrochemical properties. However, the low yield of detonation ND is also a major drawback. Considering the analogy of the D_2O in a nuclear reactor, the role of liquid in the detonation was usually explained as a coolant or energy moderator [97,110,112]. Through the water/ice can slow the over-accelerated particles as a buffer, the formation of the vapor shell is more significant in fast cooling and keeping the nanodroplets from coalescing, which leads to an increment of yield. Moreover, the detonation synthesis suffers from the undesired impurities (N, H, and O) and potential explosion risk. To eliminate such disadvantages, an advanced technology in synthesizing 0D and 1D nanomaterials has emerged featuring high-purity, controlled size & morphology, and great versatility.

2.2. Pulsed laser ablation

2.2.1. Discovery of PLA and setup

In 1960, the first functional laser was constructed using a synthetic ruby at Hughes Research Laboratory [122] based on an earlier theoretical study [123]. Since then, the laser has been widely studied for its versatile applications in a wide range of science fields. PLA is a high-power technology that transcends continuous laser devices. Briefly, techniques called “Q-switched” and “Mode Locking” were applied to produce extremely short pulse width of the laser to increase the power since the energy is equal to the average power divided by the repetition rate. Efforts have been done to lower the pulse width as short as 10^{-13} s [124], as a consequence, the power of the pulsed output laser is largely enhanced to 10^6 – 10^{14} W/cm^2 [125]. With the power in this order of

magnitude, the pulsed laser can cause superheating (> 3500 K) and non-equilibrium phase change of carbon precursors, then ceased from fast nucleation. In 1985, Smalley and his colleagues successfully synthesized C_{60} using a Q-switched $Nd:Y_3Al_5O_{12}$ laser [3]. As a milestone in the materials science history, it leads a trend in the development of PLA for the synthesis of fullerene, CNT, and semimetal-/metal-based nanomaterials.

The setup of PLA depends on the reaction media: gas or vacuum is used in a closed chamber or tube furnace, or liquid is filled in an open container. Fig. 5 illustrates three different setups: (1) a rotating target and substrate were aligned in a sphere chamber where the incident laser beam hit the target at a certain angle; (2) a pulsed laser was irradiated at the fixed target in a tube furnace; (3) laser ablates at a target that immersed in liquid for nanoparticle growth. This type of setups allows good control over temperature, pressure, gas composition, etc. The liquid medium was utilized to decrease the reaction temperature thus it generally has lower power than the solid-gaseous phase setup. It is necessary to mention that the liquid-buffering PLA usually ablate on solid substrates or dispersed insoluble particles for synthesis. Thus, the PLA is categorized in the solid-gaseous-phase reaction.

2.2.2. Nanoparticles formation mechanism of PLA and energy storage applications

PLA is a powerful technique that utilizes a high-intensity laser beam as the source to ablate the target in different media. The nanoparticles synthesized by PLA can be categorized as three types: (i) bottom-up growth of CNM (C_{60} [3] or CNT [126]) or hybrid CNM [127,128], (ii) downsize of high vaporization-temperature materials (metal nanoparticle [60,129], oxide nanoparticle [130], semiconductor quantum dot [131]), (iii) laser-induced photochemical synthesis from solution (metal nanoparticles [132,133], nitride [133]). The bottom-up method always uses gaseous-phase as the medium, while the other two usually take place in a liquid-phase.

Based on previous PLA works, Zeng [134] has summarized that the nano-/micro-second laser generates vapor and plasma due to its higher power, while millisecond (low-power) laser mainly produces nanodroplets as the initial cores. The two types of cores were also ascribed to different mechanisms of nanoparticle formation: (i) the thermal evaporation mechanism (following the interaction of vapor & plasma with the media); (ii) the mechanism of explosive ejection of nanodroplets. However, this classification only focused on the power of the laser, while missing its interactions with the other two main factors: the molecular properties of the target and the medium. Therefore, the third mechanism, laser-induced photochemical synthesis, is involved which is closely related to the laser power, wavelength, and molecule absorption property.

It usually follows the thermal evaporation mechanism if a high-power laser (microsecond or shorter) was used in the atmosphere to shoot a non-soluble bulk material. That is due to all three factors: the power, absorption, and buffer have to be considered. Specifically, the thermal evaporation mechanism [135–138] is similar to the vapor-liquid-crystal ND formation, in which the power is so high that can easily vaporize almost any bulk materials. The collision of the vapor and the ambient molecules generates a large number of electrons and ions which excite their electron state that is coupled with light emission. A plume is formed as the ions ejecting away from the bulk surface perpendicularly, then the vapor dives into the pool of gas and condensed into nanodroplets. The atmosphere molecules can keep the nanodroplets in distance and interact on the interfaces. Finally, nanoparticles are crystallized and formed after cooled down. A case in point is reported by Ou [139], in which core-shell Ni-graphene nanoparticles were synthesized by a microsecond laser (max. power at 100 μs , 210 J/pulse) ablation on Ni in CH_4/He atmosphere.

In contrast, the laser-induced photochemical synthesis mechanism was proposed when a relatively low-power laser (millisecond pulse-width or longer) was used to shoot precursors which dissolved in

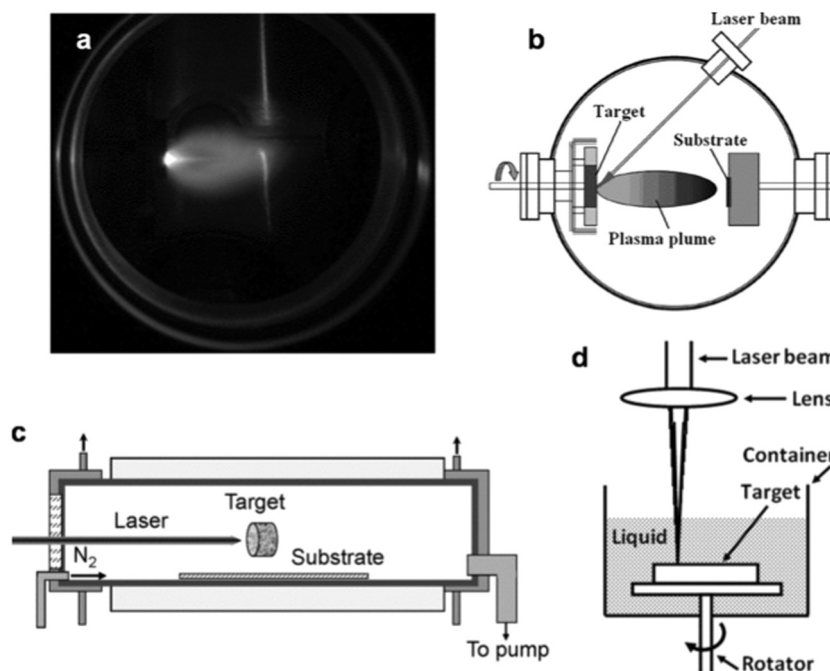


Fig. 5. (a) A plasma plume ejected from a laser-irradiated SrRuO₃ target. (b) Schematic setup of PLA in a vacuum chamber for thin-film growth. (c) PLA in a tube furnace for nanowire/nanotube growth. (d) PLA setup in liquid medium for nanoparticle growth. Reproduced with permission from [134].

liquid [132,133,140,141]. Briefly, the laser-induced photochemical synthesis is controlled by the wavelength of the laser and the light absorption & activation energy of the molecule. A photochemical reaction happens when necessary activation energy was transported from the incident light to the molecule. Following this, Pola [142] produced polymeric carbon nanoparticles by irradiating benzene and toluene in solution with an unfocused 193 nm laser (0.1 s pulse-width with an energy fluence of 100 mJ cm⁻²). Besides, Kong [143] reported an interesting synthesis by PLA of dispersed graphene & dissolved GO, in which large even-numbered carbon cluster anions C_n⁻ were formed in the absence of several odd-numbered anions in their collision process. This phenomenon may be on account of a combination of laser-induced photochemical and explosive ejection mechanism. Based on that, the increment of the observed cluster sizes with the increasing accumulation periods can be ascribed to the ions transfer process. It is reasonable to suppose that the larger the cluster is, the lower velocity it can acquire during PLA. The larger cluster has a larger cross-section, as a consequence, they can experience more collisions with residual gas. These facts indicate that the larger cluster ions require longer transfer times from the source region. Therefore, a short accumulation period can cause the loss of the large cluster ions.

The explosive ejection of nanodroplets is an intermediate synthesis mechanism between the other two [145–147]. In detail, when the power of the laser is too low, or the light absorption of the bulk/dissolved molecules is not enough to vaporize the target in an aqueous medium, the target (such as metal or alloy) will be melted into primary droplets and ejected away. The hot droplets boil the surrounding liquid and produce a high-pressure vapor shell due to the confinement effect. Subsequently, the explosion of the hot droplets forms a large number of nanodroplets that are dispersed in the liquid from coalescing. Finally, surface reactions between the nanodroplets and the molecules in the medium take place. Niu [144] reported a synthesis of Pb–PbS core-shell nanoparticles by millisecond pulsed Nd:YAG laser in liquid media. As described in Fig. 6, the composition and morphology of the end-product are governed by all three factors we have discussed.

The ultrafine nanoparticles synthesized by PLA show great promises for energy storage applications. Wang [148] reported PLA synthesized

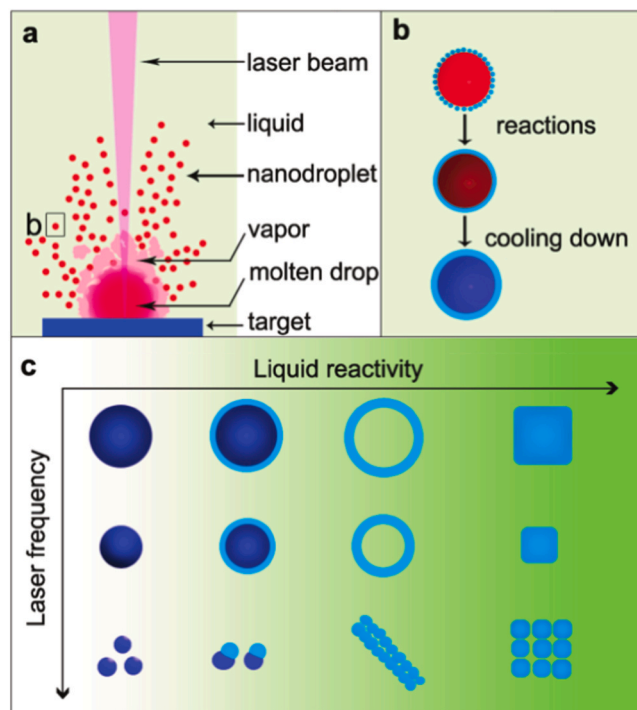


Fig. 6. Schematic diagrams of metal nanodroplet ejection and nanostructure formation in the PLA process using a low-energy millisecond laser. (a) Formation of nanodroplets. (b) Reactions of an ejected metal nanodroplet with ambient liquid. (c) Effect of liquid reactivity and laser frequency on the morphology of nanostructures formed when a Pb target was ablated in liquids. Reproduced with permission from [144].

SnO₂ nanoparticles as anode in Li-ion batteries with a capacity of 522 mA h g⁻¹ that can be obtained at 10 A g⁻¹. Nanocrystalline films grown by PLA were also reported with good performance as lithium

anode. Qin [149] synthesized Co–Co nano-films by PLA. The prepared nanocomposite exhibited outstanding cycling stability (830 mA h g^{-1} at 500 mA g^{-1} after 200 cycles) and high rate capability (578 mA h g^{-1} at $10,000 \text{ mA g}^{-1}$). Moreover, Teng [150] reported Fe_2O_3 nanocrystalline films that capable of excellent high-rate performance (510 mA h g^{-1} at a high current density of $15,000 \text{ mA g}^{-1}$) and superior cycling stability (905 mA h g^{-1} at 100 mA g^{-1} after 200 cycles).

PLA have shown extensively superiority in the bio-medical, catalyzing, energy storage & conversion applications. However, the low production efficiency and low safety highly undermine the further use for industrial applications. With that background, a striking technology has stood out for low cost, high yield, and versatile in synthesizing 0D, 1D, and 2D carbon-based nanomaterials.

2.3. Arc electric

2.3.1. Discovery of AE and setup

Since the first discovery of arc electric, it was widely applied for industrial applications, e.g. welding, smelting, lighting, plasma cutting, etc. for quite a long period. Following the synthesis of fullerene using a pulsed laser, many scientists endeavored in the formation of new carbon structures via high-power techniques. In the early 1990s, S. Iijima revealed the existence of the multi-walled and single-walled CNT via his superb transmission electron microscopy skill. Though the discovery of multi-walled CNT is controversial so far [151], it has surged a huge wave in nanomaterials research undoubtedly.

Fig. 7 shows a typical setup of an AE process, which consists of two working electrodes and a quartz window for observation in a closed chamber filled with gaseous media (liquid nitrogen, salt solution, or water are rarely used). H_2 , He, and Ar atmosphere are mostly used. The anode is a compacted rod made from a powder mixture of carbon precursor (usually graphite) and metal catalyst (Ni, Fe with Y, Mo, Co, Cr, etc.), while the cathode is made of pure graphite. After switching on the power supply, the anode and cathode are drawn close to each other to initiate the arc. Constant current or voltage is maintained by adjusting the gap to obtain a non-fluctuating arc.

2.3.2. CNM formation mechanism of AE and energy storage applications

AE is a striking technology is based on a plasma-like phenomenon when electric current breakdown a non-conductive medium. The high-temperature plasma ($2200\text{--}6773 \text{ K}$) can sublimes the carbon precursor

along with the catalyst from the anode into vapor within the millisecond's range [78]. The vapor drifts towards the cathode then deposits on the chamber wall due to the temperature gradient. To better control the structures, morphologies, and yield of the CNT by AE synthesis, extensive studies have been done for the role of various parameters such as power supply, atmosphere, pressure, catalyst & grain size, etc. Although AE can be used to synthesize graphene [152] or CNT-graphene hybrid structures [128], the majority of the studies are targeting the growth of CNT, therefore, it will be the focus of this subsection.

The power supply regulates the energy of electrons that bombard the anode, hence it is essential in the CNT formation. Three types of power sources were used in AE including direct current (DC), alternating current (AC), and pulsed arc (PA). AC was seldom used since the periodically altering polarity of AC can discharge electrons towards the cathode, as a result, the formation of CNT occurs only in the positive cycle. On the contrary, DC power supply is mostly used due to its accessibility, ease of control, and high yield.

The atmosphere is crucial for arc formation and thermo-ionic effects. During the AE, the non-conducting gas gets ionized and turns into a conductive medium due to the high-temperature-induced plasma. The ionized gas provides mass-transfer to the carbon vapor thus grants it momentum. Besides, the gases differ in their ionization potential which determines the breakdown current. Therefore, the introduction of different gases can be utilized for the growth control of CNT. Du [153] reported a CO_2 assisted AE approach that able to produce single-walled CNT with controlled length and bundle size. Furthermore, the temperature of the plasma is governed by the thermal properties of the atmosphere. Ar can generate plasma with $2200\text{--}2400 \text{ K}$, while H_2 ionized plasma leads to a temperature of around $3600\text{--}3800 \text{ K}$ [78]. Higher temperature may lead to a hetero-phase transformation, e.g. the ratio control of different H_2 concentrations (5, 12.5, 25, 50 vol%) in He can result in a quantitatively controlled number (4, 7, 9 layers) of CNT walls in a CNT-graphene hybrid structure (Fig. 8) [128]. The high specific capacitance of 350 F g^{-1} and super retention performance of almost no loss after 8000 cycles can be attributed to the high surface area and stable 3D structure formed by the instant in-situ AE synthesis.

The gas pressure determines the stability of the ions flow. It is reported that if the pressure is not in an appropriate range (differs in the type of gas), the density of gas molecules will be either too low to form a stable plasma, or so high that hinders the motion of the carbon vapor [154–157].

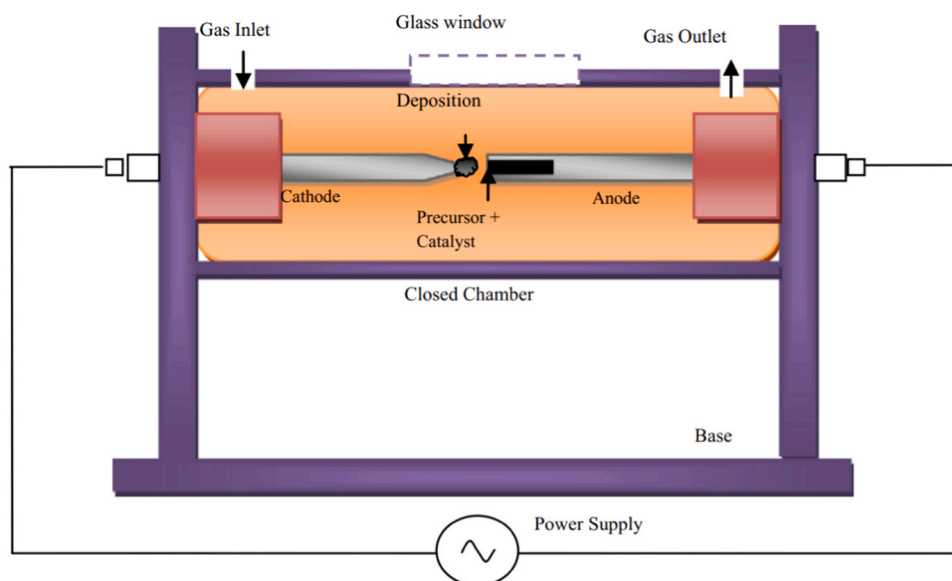


Fig. 7. Schematic of an arc discharge setup. Reproduced with permission from [78].

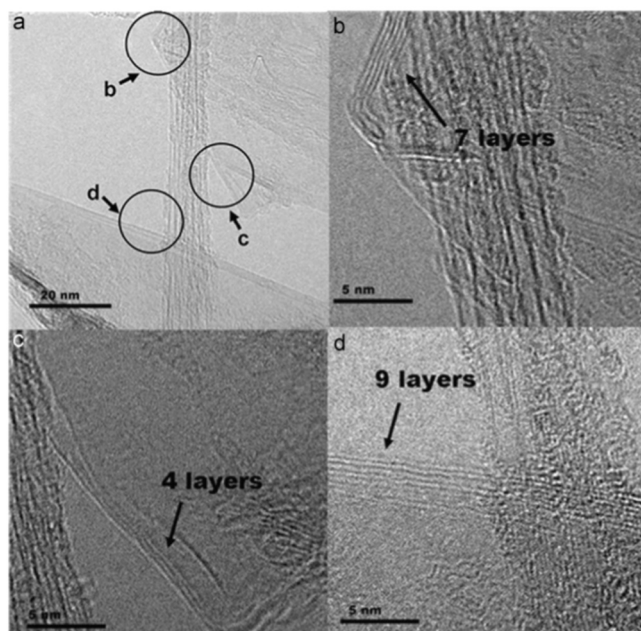


Fig. 8. High-resolution TEM images of graphene/SWNTs hybrid produced under the condition of Ni/Y/C = 4.2:1:189.6 ratio and with 12.5% (v/v) H₂ in the buffer gas: (a) The SWNTs connect two individual graphene sheets, forming a network. (b)–(d) Show the graphene sheets consist of seven (b), four (c), and nine (d) layers.

Reproduced with permission from [128].

Although few works have explained the general mechanism of CNT synthesis, theories of the CNT growth models in different phases were suggested [158,159]. A vapor-phase growth mechanism is proposed by Gamaly [158]. During the unsteady breakdown of the gas, the vaporized

carbon is granted a velocity with an isotropic distribution. Due to insufficient vapor and its momentum, it tends to form nanoparticles rather than CNT. As the current increases to a stable state, the vapor of carbon along with the metal vapor is accelerated towards the cathode, then collide onto the chamber wall in the form of nanodroplets. During the metal seeds' phase transformation from liquid to crystal, the carbon vapor keeps involving to facilitate the CNT growth. Finally, the CNT growth is terminated due to the cool down. A similar theory has also been validated elsewhere [160–163].

More importantly, the metal catalyst is irreplaceable in the growth of CNT. Low boiling temperature and the high evaporation rate is usually considered good characteristics of catalyst for CNT growth. Heer [159] suggests a liquid-phase growth model in which the precursors and catalysts are firstly vaporized and ejected towards the cathode. Since the large momentum is granted by the ionized gas, the carbon & catalyst vapor hits the cathode then scatters towards the chamber wall. During this process, the mixed vapor liquidized into nanodroplets, in which the metal catalysts serve as the seed to promote the growth of CNT (Fig. 9). It was also proposed that smaller grain sizes of precursor & catalyst have less cohesive energy [164], thus the power value required is lowered. Furthermore, experimental results show that the size of the catalyst can control the diameter distribution of CNT.

The different cathode shape can also affect the quality of the CNT. The anode usually has a smaller diameter than the cathode, which results in increased current density that favorable for the sublimation of carbon. Whereas the cathode with a larger diameter has less current density and cooler than the anode, which facilitates the fast nucleation of CNT [165]. Moreover, a strong magnetic field was applied to control the length and yield of single-walled CNT in some cases [166].

This subsection has summarized the three early HIT techniques regarding their discovery and applications. Their intrinsic high-power facilitates the fast reaction for a series of CNM and nanocomposites which is not achievable by the liquid-phase synthesis. However, many barriers are still impeding the practical employment of HIT. The

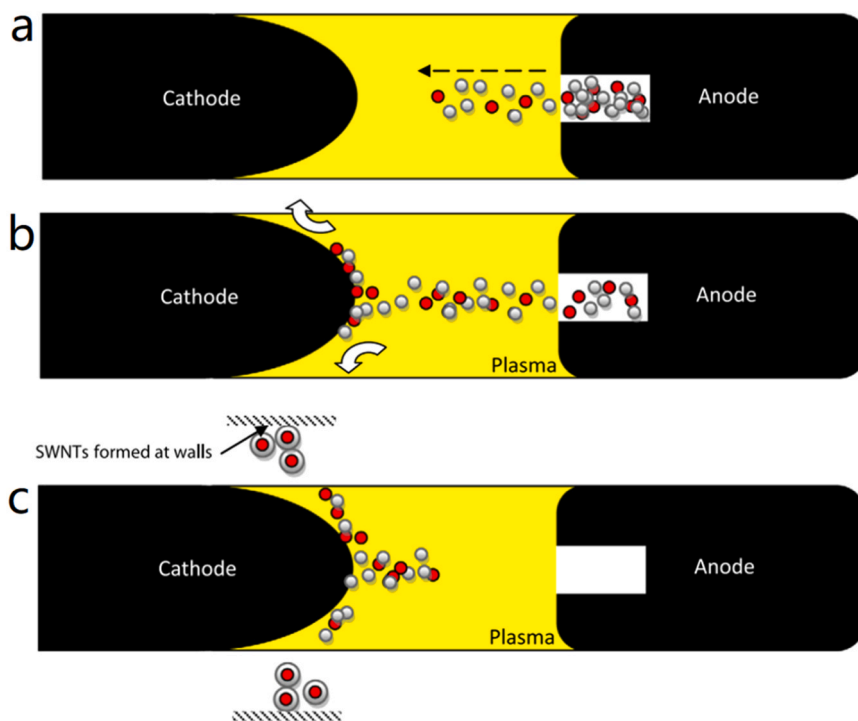


Fig. 9. Role of catalyst in the growth of CNTs: (a) the carbon vapors (gray) and metal particles (red) move toward the cathode. (b) The metal particles do not stick to the cathode and fly away from plasma due to their momentum. (c) The carbon vapors nucleate on the metal particles and form SWNT on the wall of chamber. The size of CNT depends on the size of catalyst particles.

Reproduced with permission from [78].

chambers of HIT usually require custom designs, which are time-consuming and expensive. The reproducibility of the early HIT is also a major issue. Multiple separations and purification processes are required to collect the nanomaterials within a small size range. The safety concerns of high power are also raised. Under the circumstance, two daily-life technologies stepped forward from our daily lives to pursue extraordinary applications in the synthesis of nanomaterials.

3. Hit for the synthesis of nanocomposite

With the well-developed techniques for large-scale production of CNT, graphene, and other carbon nanostructures, research of growth mechanism of CNM are fading out from the stage of materials science in the past decade. As the successors, the studies of carbon-based nanocomposites have been through an explosive increment, especially in the size-controlled and constituent-mixed fabrication by JIH and MIP. In this section, a brief history of the two old techniques will be given. Following that, the rise of JIH and MIP as frontier technologies in synthesizing nanosized metal alloy and single-atom for energy-storage and catalyzing applications will be introduced.

3.1. Joule & induction heating

The joule-heating uses high current to heat the target via a contact mode, while induction heating utilizes the eddy currents of the ferromagnetic/ferrimagnetic materials remotely. They are theoretically the same except one additional modification. In joule-heating, the AC/DC is directly from the electric power source and transport through the target. However, in induction heating, the current that travels through the sample is induced by the electromagnetic (EM) induction phenomenon from an AC powered metal coil. Therefore, we will summarize the content of these two technologies as one in this section.

3.1.1. Background of JIH and setup

In 1840, Joule first published an abstract described the phenomenon of heat generation from electric current [66]. Based on that principle, joule-heating was applied for countless civil applications including electric heaters (electric oven, hotplate, clothes iron), incandescent light bulb, welding, etc. There are two ways of joule-heating. The indirect way heats the resistive metal coil first, then transfer the heat to the target. It gains many conveniences but sacrifices the power and heating rate. Therefore, direct joule-heating was studied without the use of a metal coil or heating plate. The early practice was reported by directly applying a current through the target for food thawing in 1951 [167]. In the 1990s, scientists found that direct joule-heating can induce the amorphous-to-nanocrystalline transformation of alloy [168,169]. The use of direct joule-heating was then reported for sintering ceramic [170] and synthesizing nanoparticle-CNF composite structures such as single metal atoms [171], nanosized alloy [172], heterostructure, etc.

Typically, a direct joule-heating device consists of two electrodes connected to the sample and a power supply to provide high current through the sample (Fig. 10). Different from joule-heating, the induction device uses a metal coil to produce a high-intensity magnetic field. When the sample was put in the coil, the high current can be generated through the sample via the induction phenomenon of a strong magnetic field.

3.1.2. Nanocomposite formation via JIH and energy storage applications

JIH is a shocking technology that utilizes a large current transport through the conducting sample to generate enormous heat for the synthesis purpose. Though the non-contact induction heating is excelled in continuous processing, most of the research is using the contact-method joule-heating due to its versatile in materials and facial setup. There are two major processing routes of JIH to the best of our knowledge: (i) flash-sintering of the specimen; (ii) joule-heating of the carbon structures coated with precursors. The first route is mostly used in the ceramic industry to improve the physical & thermophysical properties and to control the phase transformation & microstructure evolution. While the joule-heating (sometimes in the name of resistance heating or carbothermal shock) is focused on the synthesis of nanoparticles-CNM composite by applying a high current through CNF [173], reduced graphene oxide (rGO) [174,175], CNT [176,177], carbonized wood [53], etc.

Flash-sintering takes advantage of the high thermal conductivity and good thermal shock resistance of selected oxide [178], nitride [179], fluoride [180], which are milled into a mixture of microparticles, then pressed to a die. The traditional sintering process takes hours in a hot furnace, sometimes combined with an applied current due to the severe conditions required [181,182]. However, the flash-sintering can be highly efficient with highly increased power. Muccillo [183] applied a flash joule-heating treatment on a mixture of ZrO_2 - Y_2O_3 with DC/AC only. The usually hour-long process was done in 90s, which shows great potential for fast-heating applications.

Wang [184] recently reported a fast-heating technology based on joule-heating for synthesizing and sintering solid-state electrolyte within 10 s (Fig. 11). The carbon paper heating elements can largely increase the max temperature limited by the Pt electrodes. High heating & cooling rates of about $10,000\text{ }^\circ\text{C}/\text{min}$ and high sintering temperatures as high as $3000\text{ }^\circ\text{C}$ thus were achieved. The as-prepared samples possess the highest reported values for planar garnet-based solid-state electrolytes with a critical current density of $3.2\text{ mA}/\text{cm}^2$ and excellent cycling stability of $> 400\text{ h}$ ($0.2\text{ mA}/\text{cm}^2$). The reason for the high performance is that the short sintering time can prevent the volatile evaporation (lithium loss), it can also reduce undesirable interdiffusion and segregation of detrimental impurities & defects at the multilayer interfaces and grain boundaries, respectively.

To explain the mechanism of the flash-sintering, Dong [185] has assumed a three-step mechanism including micro-arc welding, electric resistance welding, and diffusion-welding. The current spontaneously

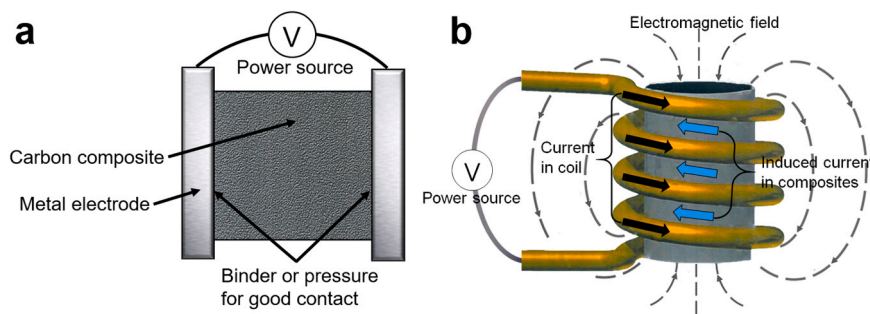


Fig. 10. Schematic of the (a) Joule heating setup and (b) induction heating setup.

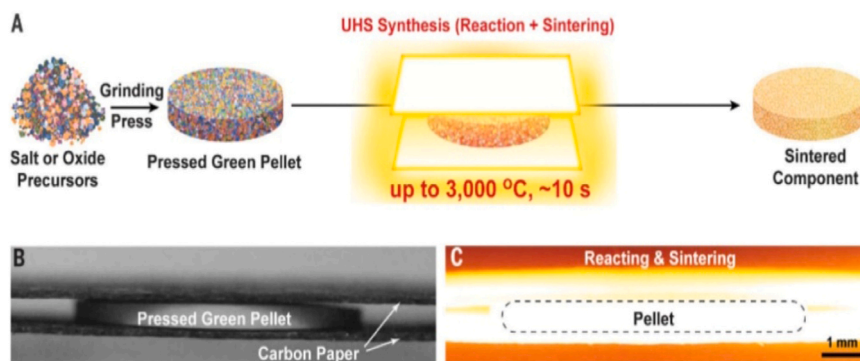


Fig. 11. Rapid sintering process and setup. (a) Schematic of the joule heating synthesis process, in which the pressed pellet of precursors is directly sintered. Photographs of the joule-heating sintering setup at room temperature without (b) and with (c) applied current, in which the closely packed heating strips provide a uniform temperature distribution.

Reproduced with permission from [184].

choose the path with the least resistance initially, thus the high-temperature micro-arc can induce the melting. As a consequence, the contact points within the path are formed and the on-path particles are welded. Following fast welding, the resistance-heating mechanism predominates the off-path particles due to the exceeded current & voltage pulse. The coalescing between particles was achieved. Finally, the diffusion-welding mechanism leads the flash-sintering process, which results in the vast metallurgical phase combination by accelerated mass transport. The specimen behaves like a semiconductor with a small bandgap due to the non-linear increase of the conductivity.

As a modified joule-heating technology, carbothermal shock synthesis rises for carbon-based nanocomposite synthesis in recent years. In this route, carbon-based substrates were used as the heating elements (same as a resistance heating wire) due to their conductivity, porosity, and stability under high temperature (~ 3000 K). Among various CNM, CNF has proved the excellence in the applications of sensing [186], catalyzing [187], energy storage [188,189], etc. for its inexpensive & mass synthesis, high-mechanical stability, and high conductivity. These unique properties make CNF an ideal candidate in flowing through a current to grow the desired morphology of the nanoparticles. Yao [171] reported a JIH synthesis of CNF-X (X refers to Pt, Ru, or Co single atoms) nanocomposites at 2000 K following periodic on-off heating. The atoms were stabilized due to the high-current shock within 55 ms, which

provides excessive activation energy. In principle, the high supersaturation of the vapor rapidly nucleate, then form large numbers of single atoms (Fig. 12). Under the circumstance, the thermodynamically favorable metal-defect can anchor the atoms onto the CNF surface. Besides, multiple substrates such as carbon, C_3N_4 , and TiO_2 can also be applied as a general route for single-atom manufacturing.

Rather than synthesizing single-metal composite, the joule-heating of CNF can incorporate multiple immiscible elements into a single nanoparticle. The same research group proposed a general route for alloying up to eight elements into single-phase nanoparticles via rapid joule-heating at a high heating rate of $\sim 10^5$ K/s [190]. It is hypothesized that the metals were liquidized into nanodroplets, and actively travel around during the heating. Furthermore, a particle-dispersion mechanism was presented, in which a catalytic-driven reaction: $C + O^* \rightarrow CO\uparrow$ was given where O^* denotes surface-bound residual oxygen. The release of CO creates a large number of defects while different metal nanodroplets coalescing each other and fusing onto the defects as an alloy. The small cluster size ~ 5 nm can be ascribed to the faster exposure time, while a prolonged process may result in a higher order of coalescent due to the punctuated thermodynamic equilibrium.

CNF has shown considerable referential importance in joule-heating for different nanocomposites. However, the mass loading of nanoparticles is limited due to the inferior surface contact between 1D CNF

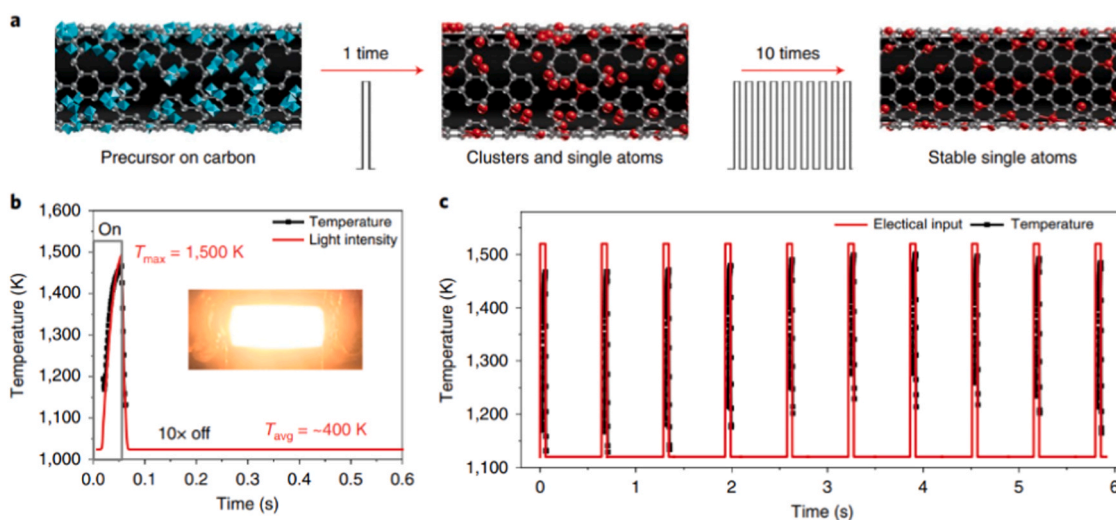


Fig. 12. Carbothermal shock synthesis of high-entropy atomic nanoparticles on carbon supports. (a) Microscopy images of micro-sized precursor salt particles on the carbon nanofibers support before the thermal shock, as well as the synthesized, well-dispersed nanoparticles. (b) Sample preparation and the temporal evolution of temperature during the 55 ms heating.

Reproduced with permission from [171].

and liquidized precursors. Moreover, the elementary substance is disfavored due to the catalytic-driven reaction requires surface-bound residual oxygen. Therefore, rGO nanosheets [174] were utilized as a high binding-energy, surface-rich substrate for a joule-heating that lasts for 30 s. Different from CNF, the mass defects on rGO can effectively trap liquidized elementary substance in long-time heating without loss, which results in an increased mass loading of 2.5 mg cm^{-2} (Fig. 13). The stabilized Si, Sn, and Al particles were in a small size distribution predominantly between 10 and 15 nm. Hence, the small size and the uniform distribution of the active materials lead to an anodic capacity of 1165 mA h g^{-1} after 100 charge-discharge cycles.

Other than the well-designed CNF or rGO mats, carbonized biomass was also used as an environmental-friendly scaffold for JIH synthesis. Yang [191] reported a facial one-step high-temperature JIH synthesis for a novel catalyst structure, in which carbonized wood was soaked with Fe (NO_3)₃, $\text{Co}(\text{NO}_3$)₂, and triethylphosphine precursors. It takes advantage of the different vapor pressure of Fe and Co at high temperature to synthesize CoFeP_x -Fe core-shell nanocatalysts via a JIH technique. The low tortuosity channels (10–50 μm) of the 3D wood can provide rapid O_2 diffusion pathways and abundant binding sites for the nanocatalysts. The channel-rich structure and in situ Fe coating ($\sim 2 \text{ nm}$) synergistically enhance the catalytic and durability of the composite for oxygen evolution reaction.

JIH mentioned above usually requires adhesion between the sample and the electrodes to promise good contact. However, the binder lowers convenience, even eliminates the feasibility of mass-production. Given that, a skillfully roll-to-roll JIH production was demonstrated by Liu [192] to overcome the contact issues. In this report, graphene film was continuously fabricated by JIH from rGO film. It paves a road to a time-saving, energy-efficient, and cost-effective heating method for potential scaled-up synthesis of CNM-nanoparticle composites.

As an old method, joule heating has evolved from a common ceramic-sintering technique to an exquisite carbon-metal bonding technology. The above-mentioned studies illuminate the bright future of JIH synthesis of well-designed solid-state and carbon-nanoparticle composites.

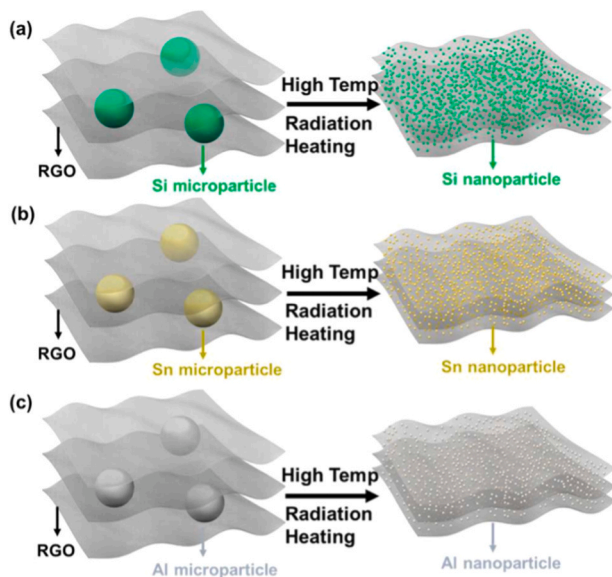


Fig. 13. Schematic illustrating a new nanoparticle synthesis methodology used for battery applications. (a) Pristine Si microparticles ($\sim 2 \mu\text{m}$) within rGO is transformed into Si nanoparticles ($\sim 10 \text{ nm}$) by a thermal shock treatment at $\sim 1800 \text{ K}$ for 30 s. The methodology also can be used to synthesize other anode composites with (b) Sn and (c) Al. The shortest radiative heating time required to transform microparticles to nanoparticles is $\sim 1 \text{ s}$, which is validated using the Sn microparticle rGO films.

Reproduced with permission from [174].

3.2. Microwave-induced plasma

3.2.1. Background of EM microwave and setup

In 1888, H. Hertz demonstrated the existence of radio waves using a spark gap radio transmitter. Since then the wave theory of light had been firmly established. In the late 1930s, the first microwave vacuum tube has been developed for low power microwave communication. Later research was mainly carried along with the development of radar. It was found that the radio waves at microwave frequencies had excessive power losses during World War II. Soon after that, the heating effect of a high-power microwave beam was accidentally discovered in 1945 [67]. From the late 1970s, the microwave oven was generally used as kitchen appliances.

Among all HIT, the setup of MIP is the simplest, which can be bought in any supermarkets normally for less than a hundred bucks. It consists of a non-ionizing EM radiation generator and a microwave-shielding case (built-in stirrer and venting inlet/outlet, see Fig. 14). There are two kinds of microwave synthesis: solvo-microwave and solid-microwave. The commonly used solvo-microwave usually requires the precursor dissolved electric dipole medium (water or organic solvent). Due to the high-frequency (2.45 GHz) alternating electric field applied by the microwave, the dipole molecules will try to align themselves with the alternating electric field. Hence the rotation of the molecules disperses energy as heat to facilitate the reaction. To avoid misunderstanding, the MIP synthesis discussed below is referred to the solid-microwave technology.

3.2.2. Nanomaterial formation via MIP and energy storage applications

MIP is a dazzling technology that utilizes EM wave radiation in the microwave-frequency region to irritate a solid sample. A microwave always interacts with matter in three pathways: reflection, transmission, and absorption. The reflection and absorption are the main causes of MIP. In certain circumstances, the reflection or/and absorption is so strong that may induce a high-temperature plasma, thus the sample was ablated and heated continuously. The sever heating effect can be ascribed to the dipolar-effect polarization, Maxwell Wagner polarization, eddy-current loss, etc [193].

Metals [194] usually have an extremely high reflection coefficient of broadband of EM wave including microwave. The metal-induced high reflectivity is due to the charge density created by the microwave exceeds the electrical potential of the metal particles, which results in the formation of a continuous arc. As a consequence, the metal particles were rapidly heated into liquid, even vapor as catalysts in the growth of CNT [195,196], which also causes a rapid energy loss of the microwave. In this case, the microwave irritation was almost reflected rather than absorbed. The work published by Chris [196] well validates this route using a microwave plasma method to grow aligned CNT under C_2H_2 and reducing vapor (Fig. 15). The CNT grows rapidly when the nucleation of catalytic cobalt initiates in a constant rate around 100 nm/s , while it decreases sharply after the cobalt particles were fully encapsulated. The diameter and length of CNT are highly dependent on the size of the cobalt particles. Besides, metal compounds such as oxide [197], nitrate

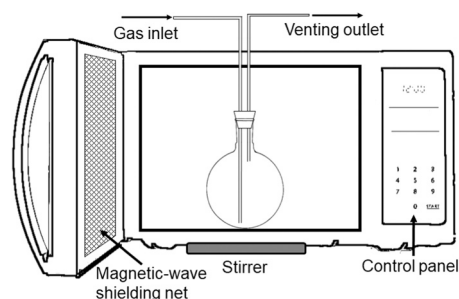


Fig. 14. Schematic of microwave setup.

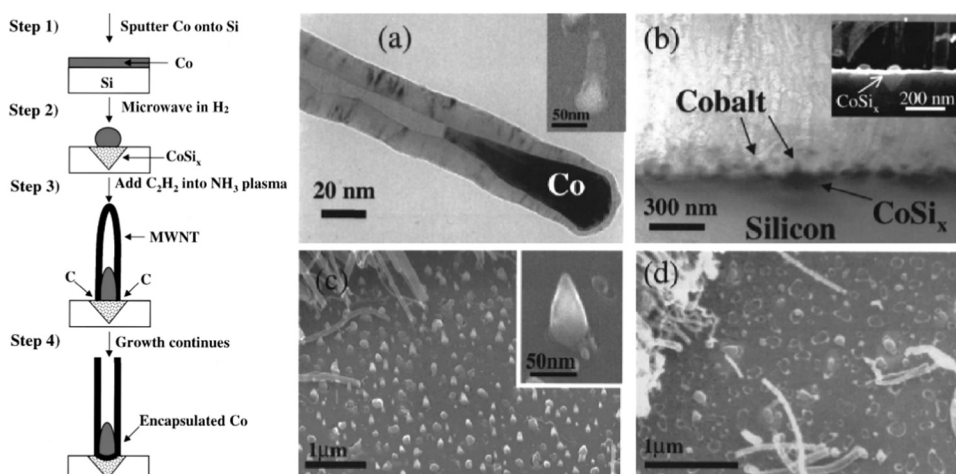


Fig. 15. Left illustration: schematic of the proposed four-step growth model. (a) TEM micrograph of a cone-shaped cobalt particle fully enclosed within one end of the multi-walled CNT. The inset shows a nanotube after 10 s (b) A cross-sectional TEM image of an aligned multi-walled CNT film. The inset shows aligned multi-walled CNT film. (c) SEM image of the “scratched” surface of a nanotube film grown for 1 min. The inset is a close-up of the cone-shaped cobalt particles left of the surface. (d) An SEM image of the “scratched” surface of a nanotube film grown for 10 min. Reproduced with permission from [196].

[198], etc. can also effectively reflect microwave in MIP synthesis since they might be reduced to metal in the presence of reducing gas or carbon. Therefore, this violent microwave reflection can be used in improving the adhesion [199], fast welding [200], forming composites [201] between metal compounds and the carbon-based materials.

Though the metal-reflection-based MIP offers an alternative way for CNT growth, the strong reflection can block the pathway of the microwave that may lead to severely inhomogeneous heating. To improve the stability of microwave heating, a metal-free route with porous carbonaceous micro-cluster was exploited such as GO [202], rGO [203–205], intercalated graphite [206], activated carbon [207], etc. Among these, graphene-based structure inherits efficient microwave absorption from graphene due to their high dielectric loss and interface-polarization [208]. Moreover, the oxygen-containing bonds may contribute to the permittivity, which is part of the absorption coefficient of the microwave [209]. Zhu [210] has demonstrated the homogeneous heating of GO by a 1 min microwave treatment followed with KOH activation. The as-prepared rGO possesses high powder conductivity of 500 S/m, a C/O atomic ratio of up to 35, and high content of sp^2 bonded carbon, which leads to a high specific capacitance. Despite the oxygen-containing bonds were mostly reduced, the slow heating rate and low exfoliating-degree of pure GO limit its potential as a fast and efficient synthesis method.

As evidenced by Hu [211], pure GO micro-flake exhibits little temperature variation and volume expansion under microwave irradiation.

However, when GO was mixed with 5% GT (graphene from thermal-expansion), it could trigger MIP which results in a remarkable volume expansion within 10 s. This an avalanche-like phenomenon can be explained by the improved absorption of porous graphene (micro-/mesopores facilitates the decrease of the effective permittivity and achieves impedance match [212,213]), which stimulating the reduction of adjacent GO (Fig. 16). In brief, the GO flake might be reduced via slow heating under microwave irradiation, however, most of the graphene layers stay stacked. In other words, a high-temperature MIP is non-attainable for individual GO micro-flake without the addition of high-dielectric materials.

Generally, the metal-triggered MIP or the graphene-induced microwave heating can be ascribed to a reflection- and absorption-dominating mechanism, respectively. As part of the EM wave shielding effects, either of the two mechanisms is inadequate for an ideal MIP synthesis. Xu [203] reported a high-temperature MIP synthesis of rGO micro-clusters deposited with a series of metal nanoparticles (Ru, Pd, and Ir). The high and homogeneous microwave absorption is achieved simultaneously due to the combination of rGO and metal precursors (Fig. 17). As a consequence, it realizes a rapid temperature rise to 1600 K in just 100 ms, which results in micro-rGO clusters deposited with nanoparticles of ~ 10 nm. MIP was also utilized as a powerful technique in ultrafast preparing nanocomposites for energy storage applications. Kim [214] have synthesized a silicon-graphene nanocomposite using a commercial microwave. The electrochemically exfoliated graphene is

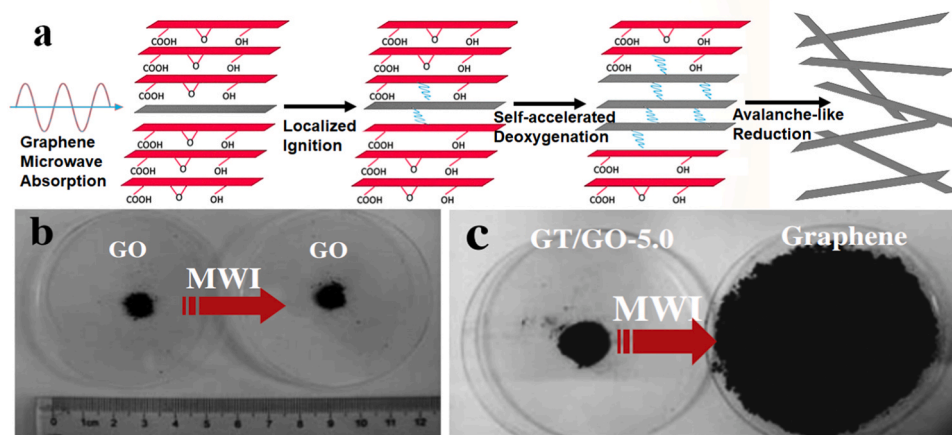


Fig. 16. (a) Illustration of the graphene-triggered reduction. Photographs of GO (b) and a GO-graphene mixture (c) before and after MW irradiation, showing the negligible response of GO to microwave irradiation and the strong influence of graphene on the reaction. Reproduced with permission. Reproduced with permission from [211].

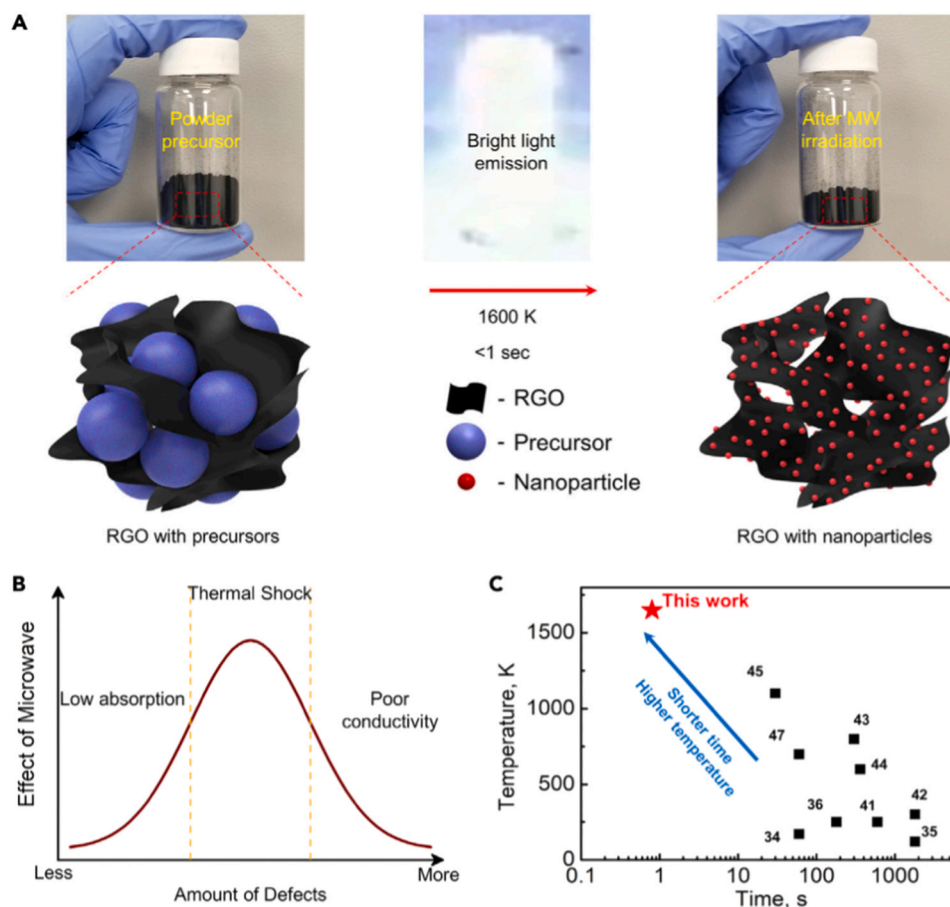


Fig. 17. Schematic of the microwave irradiation for nanoparticle synthesis (a) Photos and schematics of the rGO loaded with precursor before (left) and after microwave irradiation (right), respectively. (b) The effect of defects on the thermal shock effect, showing that the thermal shock effect only occurs when there is both good microwave absorption and good thermal conduction. (c) Comparison of heating time and temperature between this work and previous studies using microwave irradiation. Reproduced with permission from [203].

used as a novel microwave susceptor to synthesize the fine silicon particles coated with oxide layer. The as-prepared nanocomposite exhibited a reversible capacity of 1744 mA h g^{-1} at a current density of 0.1 A g^{-1} and 662 mA h g^{-1} at 1.0 A g^{-1} after 200 cycles.

As the development of MIP technology, metal precursors were coupled with GO/rGO for a uniform and efficient nanoparticle synthesis [215–219]. However, the MIP efficiency of these composites is limited due to the agglomeration caused by the oven-dried treatment. Moreover, the freeze-dry without a crosslinking treatment can also lower the MIP efficiency since the ordered porous structure could not absorb microwave as a bulk [220]. Therefore, an advanced structural-enhanced absorption of microwave was studied to further extend the limits of MIP technology.

3.2.3. Structural-enhanced absorption for MIP and energy storage applications

The integration of metallic and rGO micro-flake excels either of the individuals for MIP synthesis. However, Li [221] indicated that a particular macroscopic structure without the use of high dielectric materials may trigger a sharp increment of microwave absorption. Thus, the absorption properties of carbon fibers with and without pores were studied and stimulated, which suggests that the porous carbon structure exhibit a much better EM wave absorbing properties over a wide frequency range. It was suggested that the relatively large pores with sizes of $0.1\text{--}3 \mu\text{m}$ inside the fiber could allow multiple reflections at dihedral angles, which provides additional the propagation pathway of the microwaves [222]. Moreover, Yusoff [223] proposed that a geometrical effect might completely cancel the reflection on the air-object interface when the thickness of the object satisfies the equation: $d = n\lambda m / 4$ ($n = 1, 2, 3, \dots$). Therefore, it is supposed that evenly distributed pores with appropriate sizes can induce a dramatic microwave absorption

effect.

To further explore the structural-enhanced absorption mechanism, Zhang [224] demonstrated a precise structural control by tuning the pore size of polymeric graphene foam (range from several micrometers to tens of micrometers). The EM shielding tests show that a polymeric graphene foam can effectively absorb EM wave in a wide range of frequency (2–18 GHz). In addition to the pore-absorption theory, the absorption-induced plasma of graphene foam can also be ascribed to the resistance–inductance–capacitance coupled circuits and time-varying EM-fields-induced current [225,226], which may cause a plasmonic breakdown under adequate microwave intensity. Although the uncompressed graphene foam has a relatively low real-permittivity, the plasma inducing efficiency is high since it possesses a very small reflection loss at 2.45 GHz (Fig. 18). In detail, when the microwave was reflected within the metal walls in MIP synthesis, as a consequence, the graphene foam will absorb the energy in triggering the plasma rather than induce additional reflection. This prospective study summarized the multiple mechanisms of polymeric graphene, which paves a way for the universal applications of porous bulk-structure in MIP.

To pursue the crystal-size limit of MIP technology, the structural-enhanced microwave absorption and the high-dielectric reflection were both applied in the same study. Fei [227] reported a MIP treatment of the nitrogen-doped graphene foam decorated with metal atoms (Co, Ni, Cu). The amine-functionalized graphene foam was prepared by a three-step “hydrothermal foaming-precursors immersing-freeze drying” treatment. A unique 3D polymeric graphene foam introduces the structural-enhanced microwave absorption to the system, while the transition metal precursors contribute to the high-dielectric reflection. As a result, the synergistically worked effects enable super-fast incorporation of single atoms into the graphene lattices within 2 s (Fig. 19a). The finely distributed atomic metals bonded on graphene foam lead to

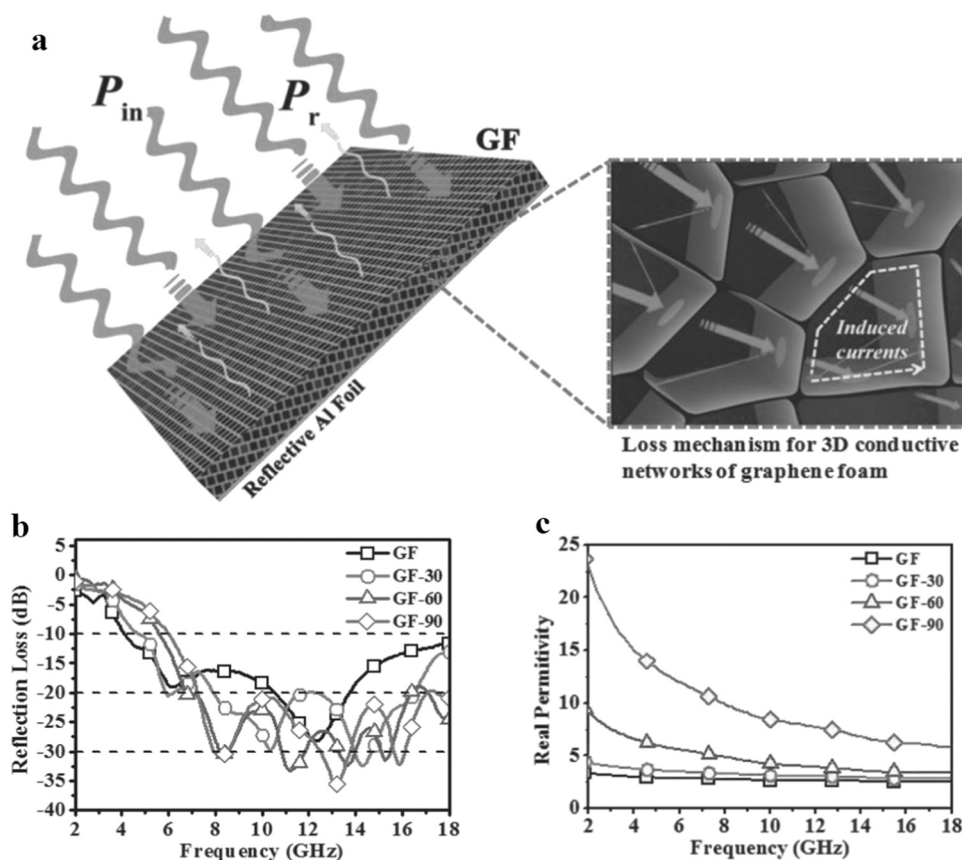


Fig. 18. (a) Schematic representation of the MA mechanism for the GF, (b) the reflection loss curves for the GFs under different compressive strains in the range 2–18 GHz. (c) Real parts of the complex permittivity of the GFs in the range 2–18 GHz. Reproduced with permission [224].

high catalytic activity and long cyclic stability compare to other works.

High energy-consuming industries contribute to the imbalance of current ecosystems, therefore, carbonized biomass [228] can bring a record-breaking low energy consumption of the whole synthetic processes. Zhong [220] proposed a rapid MIP synthesis of wood-metal oxide nanoparticles composite. The moderate electronic conductivity to the MIP and of the channel-rich property (diameter around 50 μm) carbonized wood contributes to the structural-enhanced microwave absorption which guarantees the rapid heating of the overall material (Fig. 19b–d). The temperature of the wood jumps to 2200 K in 4 s (~ 550 K/s) then stabilizing to 1400 K, which breaks the large precursor particles into evenly distributed metal oxide nanoparticles (~ 11 nm). The exploitation of biomass-based MIP method offers a green and energy-saving route for the large-scale synthesis of metal oxide nanoparticles.

Microwave has been widely used as a versatile approach that can open a new chapter for the rapid processing of a wide range of nano- or atomic-scale materials beyond the thermal equilibrium limitations. Currently, tentative efforts have been made in plasma-calcinating graphene-metal mixtures. However, the mechanism of the structural-enhanced MIP remains unrevealed. Further exploration of the solid-gaseous phase MIP may lead to a facial, and energy-efficient synthesis method.

4. Comprehensive comparison

After closely looked back at the origins and recent progress of HIT, a comparison was made in Table 1 considering the reaction time, maximum temperature, heating rate, pressure, customize flexibility, particle dispersity, energy consumption, cost, and safety.

Since the emerging of C_{60} , many kinds of CNM with designed

molecular structure, tunable sizes, regulated chirality, and controllable layers have been synthesized by the early HIT. The pros and cons of these technologies are listed below:

- (1) Detonation possesses a short reaction time, high heating rate & temperature, and exclusive high pressure that drive the thermo-kinetic only tends to grow 0D CNM such as ND [161]. The detonation ND shows limited potential in energy storage & conversion applications due to its lowered specific surface of sp^3 carbon structure. However, the ND can be produced at a low cost with non-toxic nature which shows great potential in biomedical applications. Problems remain that the undesired H, N, O elements cost a lot during purification and make the growth mechanism even more sophisticated. More importantly, the risk of explosion during storage and transportation is severely limiting its further study.
- (2) PLA shows its superiority in growing 0D fullerene and 1D CNT due to its high-energy laser can ablate almost any materials for the synthesis purpose. More than that, it is flexible in either gaseous or liquid medium, which facilitates the PLA in synthesizing numerous nanomaterials such as quantum dot, metal, alloy, oxide, nitride, etc. Carbon precursors can be easily mixed with catalysts to produce hybrid or heterogeneous nanostructures that may provide new blood for a series of research fields especially in energy storage applications. However, the high-power pulsed laser is very dangerous in accidental exposure. The pulsed laser and relevant protection devices are costly. Moreover, relatively low product yield is one of the main disadvantages of PLA.
- (3) AE excels other HIT in growing CNT, CNT/graphene, and fullerene-CNT hybrid structures due to its high temperature. The

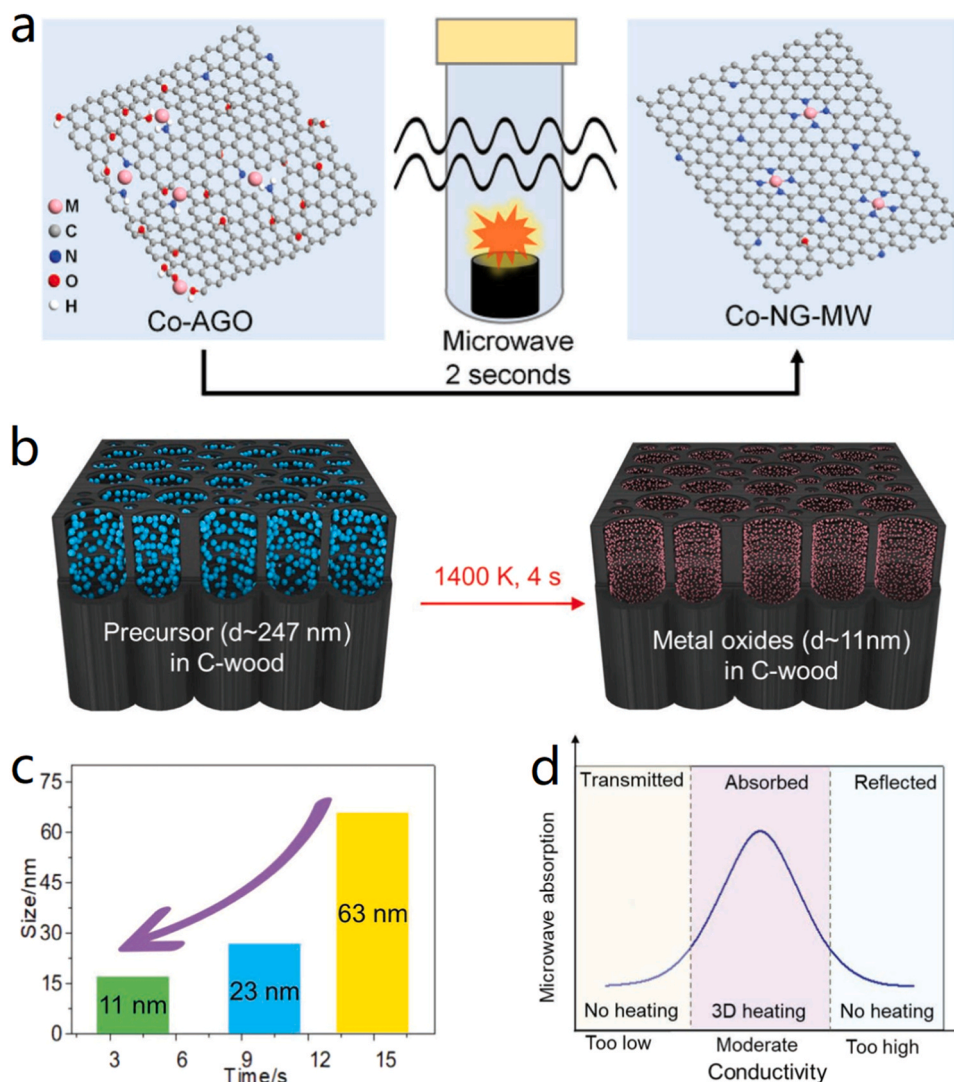


Fig. 19. (a) Schematic illustration of preparation route to Co coated nitrogen-doped graphene. (b) Schematic of metal oxide nanoparticles fabricated within the carbonized-wood substrate by the microwave treatment at ≈ 1400 K for 4 s (c) Average nanoparticle size as a function of the heating duration. (d) The effect of electronic conductivity on the microwave coupling and the resulting heating effect of carbonized wood. Reproduced with permissions from [220,227].

Table 1

Comparisons of HIT technologies in synthesizing nanomaterials.

	Detonation [1–3]	Pulsed laser ablation [5]	Arc-electric [4]	Joule & induction heating	Microwave-induced plasma
Reaction Time	0.2 μ s–1 ms	Minutes to tens of minutes	Seconds to tens of minutes	55 ms–minutes	100 ms–15 s
Temperature (K)	3000–4000	~ 3500	2200–6773	~ 3273	~ 2200
Heating rate ^a (K/s)	4×10^{10}	10^8	8.5×10^6	10^5	1.6×10^4
Pressure (kPa)	2×10^{10} – 3×10^{10}	Vacuum– 1.01×10^3	Vacuum–133	1.01×10^3	1.01×10^3
Customization Flexibility	Low	High	Low	High	High
Energy Consumption	High	High	Medium	Low	Low
Cost	High	High	Medium	Low	Low
Safety	Low	Low	Medium	Medium	High
Mass-Production Feasibility	Medium	Low	High	High	High

^a Calculated based on the reported reaction time and temperature, may vary due to the deviation.

size, layers, and constitutions of the CNM can be easily controlled by adjusting the ingredient of the anode, atmosphere, etc. Different from the detonation method, AE is free from undesired elements, thus high-purity nanomaterials can be generated. In addition, the large-scale production of CNT (kg per day) can be achieved with a lab-grade instrument since its short reaction time. Previously, AE were focused on the synthesis of CNT/graphene-based electrodes for supercapacitor applications since

the specific capacitance is related to the pore structures and surface area. The large-scale, high quality of AE-synthesized carbonaceous nanostructures e.g. CNT/graphene with metal compounds may provide a bright future in the applications of energy storage & conversion. On the other hand, the graphite anode could be consumed by the arc results in an unstable arc or interrupting the continuous production. Besides, the catalyst can be embedded in the product, which is hard to remove and

requires additional purification processes [229]. The further exploration of the CNT surface modification and heterostructure formation will lead to a way to better control their properties.

The past decade has witnessed an explosive growth of the studies of JIH and MIP, which outstand in the synthesis of CNM embedded with nanoalloys, nanocrystals, high-entropy nanoparticles, single-atoms. The following advantages and disadvantages should be taken into consideration:

- (4) JIH offers the most homogenous heating among HIT due to its heating mechanism. Its short reaction time and high heating rate enable fast vaporization and nucleation of the metal precursors, as a consequence, single-atom particles can be formed on the carbon scaffolds. JIH is flexible in the medium selections and sample preparations. It can be coupled with the multi-composition powder pressed into bulk for solid sintering, or with CNM coated with precursors for nanoparticle depositing. Generally, JIH offers a practical synthesis route with high customization flexibility, low energy consumption, medium cost, and high safety. However, the contact between the sample and the electrode suffers from the low thermal-stability. Although this problem can be prominently relieved by replacing the Pt with carbon paper, the pressure applied to the sample could be a tricky parameter which swings between the good contact and shape change. Besides, the target of JIH are limited to solid carbon scaffolds (usually CNF or graphene mats) loaded with temperature-resistant precursors on the surface. However, the high performance in variety of applications such as EM shielding, catalysts, and energy storage & conversion are related to good pore structures along with high surface area.
- (5) MIP owns superiority in size and distribution control in synthesizing carbon-metal nanocomposites due to its medium temperature and heating rate compare to JIH. It has a low energy consumption, ease of customizing, scalable-production potential, and the highest safety among all HIT. Moreover, the low cost and easy operation facilitate the MIP research of newly established labs. However, the disadvantages of MIP lays in the limitations of the target. Materials with weak microwave absorption are not favorable for MIP. Besides, the inhomogeneous heating induced by the structural-enhanced microwave absorption is jeopardizing the quality and repeatability of the nanocomposites.

5. Conclusions and outlook

This article provides an overview of the early HIT in growing a series of CNM, and tries to elucidate the fundamental mechanisms among the opposing arguments. Recent advancements of the lately raised JIH and MIP were also introduced to exhibit their promising potential in generating a variety of advanced nanocomposites. Although the studies in each of HIT have demonstrated their excellence, a remark to sum up all these synthetic technologies have not been made yet. Therefore, a general understanding of HIT for interdisciplinary research was offered. The perspectives and directions are listed below:

- (1) The early HIT such as detonation and AE have low flexibility in sample selections, high media requirements, and low customization flexibility, thus they are not suitable for synthesizing a great diversity of nanocomposites. Nevertheless, the well-studied industrial parameters grant them exclusive advantages in large-scale production of CNM. Further development of detonation and AE should target the purity improvement either by using new explosives, buffer media, additives, etc. or by optimizing the purification processes. Furthermore, the AE could be used to trigger an ionized vapor plasma of metals or semiconducting materials between two electrodes in batch synthesizing nanoparticles for novel metal-ion batteries.
- (2) The low safety and yield limit PLA in industrial applications. However, the adjustable spot size, power, media grant PLA vast advantages in precise control of the morphologies and structures of the synthesized nanoparticles toward new-class energy storage nanomaterials, e.g. complex core-shell, heterostructure, biomimetic, and carbonaceous nanostructures.
- (3) JIH is often used to sinter ceramics, yet a variety of materials could be applied in JIH for improved energy storage properties, such as metal-doped ceramic, metal-organic framework, max-phase precursors (C, Ti, Al, Zr, Si, V, Nb, Cr, N, etc.). Moreover, 3D polymeric graphene can be incorporated with insulating materials that cannot be sintered with JIH, e.g. ceramic, superelastic polymers, etc. in the applications of mechanical enhanced energy storage. The interconnected graphene network may provide fast heating throughout the sample which can perfectly solve this problem. Moreover, JIH can be used in liquid nitrogen or water to regulate the heating/cooling rate for a equilibrium.
- (4) As a crucial component in JIH, induction heating is seldom mentioned for nanocomposites synthesis. The remote-heating property of induction heating can rapidly promote the reaction while maintaining good porous structure, thus most of the contact issues can be avoided. In principle, only ferromagnetic/ferrimagnetic materials can be heated by the induction effect. However, the crosslinking of magnetic composites (e.g. Fe/Mn/Ni/Co with 3D polymeric graphene) inside the target can largely enhance the induction effect with desirable heating rate and temperature. This non-contact and controllable synthesis method can perfectly fill the incapability of the joule-heating in synthesizing 3D nanocomposites toward high-performance energy storage devices.
- (5) MIP transcends the rest of HIT in the overall performance with adequate reaction time, temperature, and heating rate while providing outstanding customization flexibility, safety, and feasibility for large-scale production. As discussed in the previous section, the reported literature lacks a comprehensive study on the mechanism of structural enhancement of microwave absorption. Thus, the future study of MIP should focus on the metal-oxide, nitride, sulfide, etc. with GO, X-doped graphene (X refers to N, P, B, etc.), exfoliated MAX phase flakes (M: Ti, V, Nb, Mo, etc.; A: Al, Si, Ga, etc.; X: C, N) built-in for efficient microwave-heat conversion. It's unique remotely heating mode enables a high mass loading of catalytic materials while maintaining a good 3D structure, which is perfect for the applications in novel metal ion batteries, metal-air batteries, catalysts, and EM wave shielding. Furthermore, the enormous 3D materials built by 3D printing with controllable structure and pore size can be combined with the novel in situ characterization techniques, which may facilitate the understanding of the unrevealed mechanisms. A new perception of microwave absorption, heat generation & dissipation, and electrical & thermal transport will be essential for controllable MIP synthesis.
- (6) AE can be combined with MIP in a production line since it can synthesis a series of CNM such as CNT, graphene, and CNT@graphene hybrid structures without undesired impurities. As-prepared CNM will be collected by a cyclone separator for sieving. After the suitable precursors were added, the intermediate product will be transferred to a conveyor for MIP synthesis. As a consequence, embedded active materials (such as catalysts or anode materials) from the AE will be easily turned into nanoparticles with controllable grain sizes due to high heating rate. This promising route might offer a practical route for mass-producing a variety of CN-nanocatalysts for catalyzing, pollution degradation, energy storage & conversion.
- (7) As an arising concern, the energy consumption in terms of greenhouse emission of HIT should be considered. Life-cycle assessment is a common method to analyze the environmental impacts

of technology from the perspective of energy consumption. The analysis starts with the mining of the source (graphite, metal ore, etc.) to the waste recycling of all the compositions, which gives a suggestive point for industrial production. After comparing all the GHG emissions of the processes, the most sustainable route will be provided.

To conclude, HIT are superior in synthesizing nanomaterials with controllable morphology, distinguished atomic architecture, as well as unique properties, which excels the other techniques. Be specific, the early HIT are irreplaceable in growing CNM, while the late HIT are outstanding in synthesizing carbon-nanoparticles composites. Therefore, the tremendous potential of HIT remains in store to be exploited. Further studies of HIT may pave an efficient avenue for the design and preparation of highly efficient nanostructures for catalyzing, biomedical, photovoltaic conversion, sensing, artificial tissue engineering, seawater desalination, EM shielding, and energy storage applications.

Declaration of Competing Interest

The authors declare that they have no known competing financial interests or personal relationships that could have appeared to influence the work reported in this paper.

Acknowledgments

The authors gratefully acknowledge the financial support from Ministry of Science and Technology of the People's Republic of China (2016YFA0200200), the National Natural Science Foundation of China (21421001, 51633002, and 21671176), Tianjin City (16ZXCLGX00100) and 111 Project (B12015).

Conflicts of interest

There are no conflicts to declare.

Appendix. A list of abbreviations used in this article

HIT	High-power instant-synthesis technology
DET	Detonation
PLA	Pulsed laser ablation
AE	Arc electric
JIH	Joule & induction heating
MIP	Microwave-induced plasma
CVD	Chemical vapor deposition
PVD	Physical vapor deposition
TNT	Trinitrotoluene
CNM	Carbon nanomaterials
ND	Nanodiamonds
CNF	Carbon nanofibers
CNT	Carbon nanotubes
MWCNT	Multi-walled carbon nanotubes
SWCNT	Single-walled carbon nanotubes
DC	Direct current
AC	Alternating current
PA	Pulsed arc
EM	Electromagnetic
rGO	Reduced graphene oxide

References

- [1] T. Zhang, H. Chang, Y. Wu, P. Xiao, N. Yi, Y. Lu, Y. Ma, Y. Huang, K. Zhao, X.-Q. Yan, *Nat. Photonics* 9 (2015) 471–476.
- [2] A.R. Bin Mohd Yusoff, S.J. Lee, J. Jang, G. Long, X. Wan, Y. Chen, *J. Mater. Chem. A* 2 (2014) 19988–19993.
- [3] H.W. Kroto, J.R. Heath, S.C. O'Brien, R.F. Curl, R.E. Smalley, *Nature* 318 (1985) 162–163.
- [4] S. Iijima, T. Ichihashi, *Nature* 363 (1993) 603–605.
- [5] K.S. Novoselov, A.K. Geim, S.V. Morozov, D. Jiang, Y. Zhang, S.V. Dubonos, I. V. Grigorieva, A.A. Firsov, *Science* 306 (2004) 666–669.
- [6] A. Goldstein, C. Echer, A. Alivisatos, *Science* 256 (1992) 1425–1427.
- [7] R.S. Ruoff, D.C. Lorents, B. Chan, R. Malhotra, S. Subramoney, *Science* 259 (1993) 346–348.
- [8] C. Murray, C. Kagan, M. Bawendi, *Science* 270 (1995) 1335–1338.
- [9] X. Duan, Y. Huang, Y. Cui, J. Wang, C.M. Lieber, *Nature* 409 (2001) 66–69.
- [10] Y. Huang, X. Duan, Q. Wei, C.M. Lieber, *Science* 291 (2001) 630–633.
- [11] Z.W. Pan, Z.L. Wang, *Science* 291 (2001) 1947–1949.
- [12] Y. Xia, P. Yang, Y. Sun, Y. Wu, B. Mayers, B. Gates, Y. Yin, F. Kim, H. Yan, *Adv. Mater.* 15 (2003) 353–359.
- [13] W. Ma, C. Yang, X. Gong, K. Lee, A.J. Heeger, *Adv. Funct. Mater.* 15 (2005) 1617–1622.
- [14] N.W.S. Kam, M. O'Connell, J.A. Wisdom, H. Dai, *Proc. Natl. Acad. Sci.* 102 (2005) 11600–11605.
- [15] D.W. Wang, F. Li, M. Liu, G.Q. Lu, H.M. Cheng, *Angew. Chem. Int. Ed.* 47 (2008) 373–376.
- [16] X. Liu, K. Zhou, L. Wang, B. Wang, Y. Li, *J. Am. Chem. Soc.* 131 (2009) 3140–3141.
- [17] J. Cai, P. Ruffieux, R. Jaafar, M. Bieri, T. Braun, S. Blankenburg, M. Muoth, A. P. Seitsonen, M. Saleh, X. Feng, *Nature* 466 (2010) 470–473.
- [18] M.D. Lima, N. Li, M.J. De Andrade, S. Fang, J. Oh, G.M. Spinks, M.E. Kozlov, C. S. Haines, D. Suh, J. Foroughi, *Science* 338 (2012) 928–932.
- [19] D. Deng, L. Yu, X. Chen, G. Wang, L. Jin, X. Pan, J. Deng, G. Sun, X. Bao, *Angew. Chem.* 125 (2013) 389–393.
- [20] Q. Liang, Z. Li, X. Yu, Z.H. Huang, F. Kang, Q.H. Yang, *Adv. Mater.* 27 (2015) 4634–4639.
- [21] R. Fang, S. Zhao, Z. Sun, D.W. Wang, H.M. Cheng, F. Li, *Adv. Mater.* 29 (2017), 1606823.
- [22] R. Ma, Z. Zhang, K. Tong, D. Huber, R. Kornbluh, Y.S. Ju, Q. Pei, *Science* 357 (2017) 1130–1134.
- [23] R.-W. Huang, Y.-S. Wei, X.-Y. Dong, X.-H. Wu, C.-X. Du, S.-Q. Zang, T.C.W. Mak, *Nat. Chem.* 9 (2017) 689–697.
- [24] Y.-E. Zhu, L. Yang, J. Sheng, Y. Chen, H. Gu, J. Wei, Z. Zhou, *Adv. Energy Mater.* 7 (2017), 1701222.
- [25] R. Zhang, N.W. Li, X.B. Cheng, Y.X. Yin, Q. Zhang, Y.G. Guo, *Adv. Sci.* 4 (2017), 1600445.
- [26] J. Lopez, A. Pei, J.Y. Oh, G.-J.N. Wang, Y. Cui, Z. Bao, *J. Am. Chem. Soc.* 140 (2018) 11735–11744.
- [27] Y. Yang, J. Liang, F. Pan, Z. Wang, J. Zhang, K. Amin, J. Fang, W. Zou, Y. Chen, X. Shi, *Nat. Commun.* 9 (2018) 1–8.
- [28] J. Hou, O. Inganäs, R.H. Friend, F. Gao, *Nat. Mater.* 17 (2018) 119–128.
- [29] Y. Cui, J.D. Ackerson, Y. Ma, A. Bhargava, J.A. Karty, W. Guo, L. Zhu, Y. Fu, *Adv. Funct. Mater.* 28 (2018), 1801791.
- [30] J. Han, D. Kong, W. Lv, D.-M. Tang, D. Han, C. Zhang, D. Liu, Z. Xiao, X. Zhang, J. Xiao, *Nat. Commun.* 9 (2018) 1–9.
- [31] H. Yao, X. Wang, H. Dong, R. Pei, J. Wang, Z. Li, *Ceram. Int.* 37 (2011) 3153–3160.
- [32] R. Pei, X. Chen, Y. Suo, T. Xiao, Q. Ge, H. Yao, J. Wang, Z. Li, *Solid State Ion.* 219 (2012) 34–40.
- [33] L. Zhang, Y. Huang, Y. Zhang, Y. Ma, Y. Chen, *J. Nanosci. Nanotechnol.* 13 (2013) 1129–1131.
- [34] Z. Nie, A. Petukhova, E. Kumacheva, *Nat. Nanotechnol.* 5 (2010) 15–25.
- [35] M.A. Lopez-Quintela, *Curr. Opin. Colloid* 8 (2003) 137–144.
- [36] V.G. Pol, D. Srivastava, O. Palchik, V. Palchik, M. Slifkin, A. Weiss, A. Gedanken, *Langmuir* 18 (2002) 3352–3357.
- [37] M. Berghaus, R. Mohammadi, B. Sellergren, *Chem. Commun.* 50 (2014) 8993–8996.
- [38] P. Mokarian-Tabari, C. Cummins, S. Rasappa, C. Simao, C.M. Sotomayor Torres, J.D. Holmes, M.A. Morris, *Langmuir* 30 (2014) 10728–10739.
- [39] J. Liang, Y. Wang, Y. Huang, Y. Ma, Z. Liu, J. Cai, C. Zhang, H. Gao, Y. Chen, *Carbon* 47 (2009) 922–925.
- [40] F. Zhang, X. Yang, Y. Xie, N. Yi, Y. Huang, Y. Chen, *Carbon* 82 (2015) 161–167.
- [41] Y. Liu, Z. Zeng, R.K. Sharma, S. Gbewonyo, K. Allado, L. Zhang, J. Wei, *J. Power Sources* 409 (2019) 1–5.
- [42] J. Kong, A.M. Cassell, H. Dai, *Chem. Phys. Lett.* 292 (1998) 567–574.
- [43] A. Martinez, K. Fuse, S. Yamashita, *Appl. Phys. Lett.* 99 (2011), 121107.
- [44] H. Garbacz, P. Wicziński, B. Adamczyk-Cieślak, J. Mizera, K. Kurzydowski, *J. Microsc.* 237 (2010) 475–480.
- [45] J.-J. Wu, T.-R. Lu, C.-T. Wu, T.-Y. Wang, L.-C. Chen, K.-H. Chen, C.-T. Kuo, T.-M. Chen, Y.-C. Yu, C.-W. Wang, *Diam. Relat. Mater.* 8 (1999) 605–609.
- [46] Š. Meškinis, V. Kopustinskas, K. Šlapikas, S. Tamulevičius, A. Guobienė, R. Gudaitis, V. Grigaliūnas, *Thin Solid Films* 515 (2006) 636–639.
- [47] J. Choi, T. Kim, C. Lee, D. Jeon, G. Park, S. Cho, M. Park, I. Yu, M. Iwakuma, *IEEE Trans. Appl. Supercond.* 29 (2019) 1–5.
- [48] P. Allia, M. Baricco, P. Tiberto, F. Vinai, *Phys. Rev. B* 47 (1993) 3118.
- [49] N.J. Wu, A. Ignatiev, A.-W. Mesarwi, H. Lin, K. Xie, H.-D. Shih, *Jpn. J. Appl. Phys.* 32 (1993) 5019.
- [50] G. Zhong, S. Xu, M. Cui, Q. Dong, X. Wang, Q. Xia, J. Gao, Y. Pei, Y. Qiao, G. Pastel, T. Sunaoshi, B. Yang, L. Hu, *Small* 15 (2019), 1904881.
- [51] B. Liu, R. Shi, R. Chen, C. Wang, K. Zhou, Y. Ren, Z. Zeng, Y. Liu, L. Li, *Appl. Surf. Sci.* (2020), 147961.
- [52] A. Malshe, B. Park, W. Brown, H. Naseem, *Diam. Relat. Mater.* 8 (1999) 1198–1213.

- [53] Y. Li, T. Gao, Y. Yao, Z. Liu, Y. Kuang, C. Chen, J. Song, S. Xu, E.M. Hitz, B. Liu, R. J. Jacob, M.R. Zachariah, G. Wang, L. Hu, *Adv. Energy Mater.* 8 (2018), 1801289.
- [54] O. Kordina, C. Hallin, A. Ellison, A. Bakin, I.G. Ivanov, A. Henry, R. Yakimova, M. Touminen, A. Vehanen, E. Janzen, *Appl. Phys. Lett.* 69 (1996) 1456–1458.
- [55] R. Addou, A. Dahal, P. Sutter, M. Batzill, *Appl. Phys. Lett.* 100 (2012), 021601.
- [56] J. Singh, D.E. Wolfe, *J. Mater. Sci.* 40 (2005) 1–26.
- [57] A.-S. Al-Sherbini, M. Bakr, I. Ghoneim, M. Saad, *J. Adv. Res.* 8 (2017) 209–215.
- [58] B. Movchan, *JOM* 48 (1996) 40–45.
- [59] V.N. Mochalin, O. Shenderova, D. Ho, Y. Gogotsi, *Nat. Nanotechnol.* 7 (2012) 11–23.
- [60] F. Mafuné, J.-y Kohno, Y. Takeda, T. Kondow, H. Sawabe, *J. Phys. Chem. B* 104 (2000) 9111–9117.
- [61] Y. Wu, B. Wang, Y. Ma, Y. Huang, N. Li, F. Zhang, Y. Chen, *Nano Res.* 3 (2010) 661–669.
- [62] A.G. Mikerov, in: *Proceedings of the IEEE NW Russia Young Researchers in Electrical and Electronic Engineering Conference, 2014*, pp. 1–7.
- [63] X. Xu, Y. Du, C. Wang, Y. Guo, J. Zou, K. Zhou, Z. Zeng, Y. Liu, L. Li, J. Alloy. *Compd.* 822 (2020), 153642.
- [64] R. Roy, D. Agrawal, J. Cheng, S. Gedeveanishvili, *Nature* 399 (1999) 668–670.
- [65] A. Anders, *IEEE Trans. Plasma Sci.* 31 (2003) 1060–1069.
- [66] J.P. Joule, *The Scientific Papers of James Prescott Joule*, Cambridge University Press, 2011.
- [67] T.G. Roer, *Microwave Electronic Devices*, Springer Science & Business Media, 2012.
- [68] Y. Yang, M.C. Gupta, K.L. Dudley, R.W. Lawrence, *Adv. Mater.* 17 (2005) 1999–2003.
- [69] Q. Zhao, Y. Lin, N. Han, X. Li, H. Geng, X. Wang, Y. Cui, S. Wang, *Drug Deliv.* 24 (2017) 94–107.
- [70] F. Cheng, J. Shen, W. Ji, Z. Tao, J. Chen, *ACS Appl. Mater. Interfaces* 1 (2009) 460–466.
- [71] S.C. Mannsfeld, B.C. Tee, R.M. Stoltenberg, C.V.H. Chen, S. Barman, B.V. Muir, A. N. Sokolov, C. Reese, Z. Bao, *Nat. Mater.* 9 (2010) 859–864.
- [72] C. Su, Y. Guo, H. Chen, J. Zou, Z. Zeng, L. Li, *Colloids Surf. A* (2020), 124983.
- [73] Y. He, H.-Y. Chen, J. Hou, Y. Li, *J. Am. Chem. Soc.* 132 (2010) 1377–1382.
- [74] Y. Lu, Y. Lu, Z. Niu, J. Chen, *Adv. Energy Mater.* 8 (2018), 1702469.
- [75] D.L. Fedlheim, C.A. Foss, *Metal Nanoparticles: Synthesis, Characterization, and Applications*, CRC Press, 2001.
- [76] N. Rajput, *Int. J. Adv. Eng. Technol.* 7 (2015) 1806.
- [77] A.V. Rane, K. Kanny, V. Abitha, S. Thomas, *Methods for Synthesis of Nanoparticles and Fabrication of Nanocomposites, Synthesis of Inorganic Nanomaterials*, Elsevier, 2018, pp. 121–139.
- [78] N. Arora, N. Sharma, *Diam. Relat. Mater.* 50 (2014) 135–150.
- [79] V. Pichot, M. Comet, B. Risse, D. Spitzer, *Diam. Relat. Mater.* 54 (2015) 59–63.
- [80] S. Dou, J. Xu, X. Cui, W. Liu, Z. Zhang, Y. Deng, W. Hu, Y. Chen, *Adv. Energy Mater.* (2020), 2001331.
- [81] V.V. Danilenko, *Phys. Solid State* 46 (2004) 595–599.
- [82] M. Endo, T. Koyama, Y. Hishiyama, *Jpn. J. Appl. Phys.* 15 (1976) 2073–2076.
- [83] M. Zeiger, N. Jäckel, V.N. Mochalin, V. Presser, *J. Mater. Chem. A* 4 (2016) 3172–3196.
- [84] K.S. Munir, C. Wen, *Crit. Rev. Solid State Mater.* 41 (2016) 347–366. Sc0069.
- [85] Y. Xu, Z. Liu, X. Zhang, Y. Wang, J. Tian, Y. Huang, Y. Ma, X. Zhang, Y. Chen, *Adv. Mater.* 21 (2009) 1275–1279.
- [86] J.E. Mark, *Physical Properties of Polymers Handbook*, Springer, 2007.
- [87] V.N. Mochalin, A. Pentecost, X.-M. Li, I. Neitzel, M. Nelson, C. Wei, T. He, F. Guo, Y. Gogotsi, *Mol. Pharm.* 10 (2013) 3728–3735.
- [88] M. Montalti, A. Cantelli, G. Battistelli, *Chem. Soc. Rev.* 44 (2015) 4853–4921.
- [89] Q. Zhang, V.N. Mochalin, I. Neitzel, K. Hazeli, J. Niu, A. Kontsos, J.G. Zhou, P. I. Lelkes, Y. Gogotsi, *Biomaterials* 33 (2012) 5067–5075.
- [90] A.M. Schrand, S.A.C. Hens, O.A. Shenderova, *Crit. Rev. Solid State Mater. Sci.* 34 (2009) 18–74.
- [91] J.-P. Boudou, P.A. Curmi, F. Jelezko, J. Wrachtrup, P. Aubert, M. Sennour, G. Balasubramanian, R. Reuter, A. Thorel, E. Gaffet, *Nanotechnology* 20 (2009), 235602.
- [92] S. Osswald, M. Havel, V. Mochalin, G. Yushin, Y. Gogotsi, *Diam. Relat. Mater.* 17 (2008) 1122–1126.
- [93] K. Iakoubovskii, K. Mitsuishi, K. Furuya, *Nanotechnology* 19 (2008), 155705.
- [94] V.Y. Dolmatov, *Russ. Chem. Rev.* 76 (2007) 339.
- [95] O.A. Shenderova, G.E. McGuire, *Biointerphases* 10 (2015), 030802.
- [96] K. Yamada, A. Sawaoka, *Carbon* 32 (1994) 665–673.
- [97] A.Y. Babushkin, A. Lyamkin, IV Vserossiiskaya konferentsiya “Fiziko-khimiyaul’ tradispersnykh sistem”. *Sbornik nauchnykh trudov*, 1999, pp. 125–128.
- [98] V. Danilenko, *Energoatomizdat, Moscow*, 2002.
- [99] J. Shaner, J. Brown, C. Swenson, R. McQueen, *J. Phys. Colloq.* 45 (1984). C8-235-C238-237.
- [100] M. Togaya, *Phys. Rev. Lett.* 79 (1997) 2474.
- [101] F.P. Bundy, H.P. Bovenkerk, H.M. Strong, R.H. Wentorf Jr, *J. Chem. Phys.* 35 (1961) 383–391.
- [102] V. Danilenko, *Fiz. Goreniyai Vzryv* 41 (2005) 104–116.
- [103] O. Breusov, *Khim. Fiz.* 21 (2002) 110–112.
- [104] L. Dubnov, N. Bakharevich, A. Romanov, *Industrial Explosives, Nedra, Moscow*, 1988.
- [105] A. Nesmeyanov, N. Nesmeyanov, *Princ. Org. Chem.* 2 (1974).
- [106] E.E. Lin, *Proc. Vth Zababakhin’s Read.* (1999) 679–688.
- [107] V. Anisickin, B. Derendyaev, V. Koptyug, *Fiz. Goreniya Vzryv* 24 (1988) 121–122.
- [108] V.M. Titov, V.F. Anisichkin, I. Yu Mal’kov, *Fiz. Goreniya Vzryv* 25 (1989) 117–125.
- [109] B. Vyskubenko, V. Danilenko, E. Lin, *Fiz. Goreniya Vzryv* 28 (1992) 108.
- [110] V.Y. Dolmatov, *J. Superhard Mater.* 30 (2008) 233–240.
- [111] J.R. Petherbridge, P.W. May, S.R. Pearce, K.N. Rosser, M.N. Ashfold, *J. Appl. Phys.* 89 (2001) 1484–1492.
- [112] V.Y. Dolmatov, V. Myllymäki, A. Vehanen, *J. Superhard Mater.* 35 (2013) 143–150.
- [113] L. Zhang, X. Yang, F. Zhang, G. Long, T. Zhang, K. Leng, Y. Zhang, Y. Huang, Y. Ma, M. Zhang, *J. Am. Chem. Soc.* 135 (2013) 5921–5929.
- [114] C. Portet, G. Yushin, Y. Gogotsi, *Carbon* 45 (2007) 2511–2518.
- [115] J. Xu, K. Natsui, S. Naoi, K. Nakata, Y. Einaga, *Diam. Relat. Mater.* 86 (2018) 167–172.
- [116] Y. Liu, S. Chen, X. Quan, H. Yu, *J. Am. Chem. Soc.* 137 (2015) 11631–11636.
- [117] S. Yu, J. Xu, H. Kato, N. Yang, A. Schulte, H. Schönherr, X. Jiang, *ChemElectroChem* 6 (2019) 1088–1093.
- [118] I. Kovalenko, D.G. Bucknall, C. Yushin, *Adv. Funct. Mater.* 20 (2010) 3979–3986.
- [119] K. Honda, M. Yoshimura, K. Kawakita, A. Fujishima, Y. Sakamoto, K. Yasui, N. Nishio, H. Masuda, *J. Electrochem. Soc.* 151 (2004) A532.
- [120] Q. Wang, N. Plylahan, M.V. Shelke, R.R. Devarapalli, M. Li, P. Subramanian, T. Djenizian, R. Boukherroub, S. Szunerits, *Carbon* 68 (2014) 175–184.
- [121] N. Spätaru, X. Zhang, T. Spätaru, D.A. Tryk, A. Fujishima, *J. Electrochem. Soc.* 155 (2007) D73.
- [122] T.H. Maiman, *Nature* 187 (1960) 493–494.
- [123] A.L. Schawlow, C.H. Townes, *Phys. Rev.* 112 (1958) 1940–1949.
- [124] J. Armstrong, *Appl. Phys. Lett.* 10 (1967) 16–18.
- [125] S.-W. Bahk, P. Rousseau, T. Planchon, V. Chvykov, G. Kalintchenko, A. Maksimchuk, G. Mourou, V. Yanovsky, *Opt. Lett.* 29 (2004) 2837–2839.
- [126] A. Puretzyk, D. Geohegan, X. Fan, S. Pennycook, *Appl. Phys. A* 70 (2000) 153–160.
- [127] R. Huang, W. Lu, S. Yang, *J. Chem. Phys.* 102 (1995) 189–192.
- [128] Y. Wu, T. Zhang, F. Zhang, Y. Wang, Y. Ma, Y. Huang, Y. Liu, Y. Chen, *Nano Energy* 1 (2012) 820–827.
- [129] Y. Kawakami, T. Seto, T. Yoshida, E. Ozawa, *Appl. Surf. Sci.* 197 (2002) 587–593.
- [130] S. Shinde, S. Kulkarni, A. Banpurkar, R. Nawathe-Dixit, S. Date, S. Ogale, *J. Appl. Phys.* 88 (2000) 1566–1575.
- [131] K. Anikin, N. Melnik, A. Simakin, G. Shafeev, V. Voronov, A. Vitukhnovsky, *Chem. Phys. Lett.* 366 (2002) 357–360.
- [132] R. Shukla, S.K. Nune, N. Chanda, K. Katti, S. Mekapothula, R.R. Kulkarni, W. V. Welshons, R. Kannan, K.V. Katti, *Small* 4 (2008) 1425–1436.
- [133] H. Liu, P. Jin, Y.-M. Xue, C. Dong, X. Li, C.-C. Tang, X.-W. Du, *Angew. Chem. Int. Ed.* 54 (2015) 7051–7054.
- [134] H. Zeng, X.W. Du, S.C. Singh, S.A. Kulnich, S. Yang, J. He, W. Cai, *Adv. Funct. Mater.* 22 (2012) 1333–1353.
- [135] H. Zeng, W. Cai, Y. Li, J. Hu, P. Liu, *J. Phys. Chem. B* 109 (2005) 18260–18266.
- [136] P. Liu, W. Cai, H. Zeng, *J. Phys. Chem. C* 112 (2008) 3261–3266.
- [137] H. Zeng, Z. Li, W. Cai, B. Cao, P. Liu, S. Yang, *J. Phys. Chem. B* 111 (2007) 14311–14317.
- [138] H. Zeng, X. Xu, Y. Bando, U.K. Gautam, T. Zhai, X. Fang, B. Liu, D. Golberg, *Adv. Funct. Mater.* 19 (2009) 3165–3172.
- [139] Q. Ou, T. Tanaka, M. Mesko, A. Ogino, M. Nagatsu, *Diam. Relat. Mater.* 17 (2008) 664–668.
- [140] H.-C. Kim, H. Reinhardt, P. Hillebrecht, N.A. Hampp, *Adv. Mater.* 24 (2012) 1994–1998.
- [141] R. Gokhale, V. Thakare, S. Warule, B. Lefez, B. Hannover, J. Jog, S. Ogale, *AIP Adv.* 2 (2012), 022130.
- [142] J. Pola, M. Urbanova, Z. Bastl, Z. Plzak, J. Šubrt, V. Vorlíček, I. Gregora, C. Crowley, R. Taylor, *Carbon* 35 (1997) 605–611.
- [143] X. Kong, S. Li, S. Zhang, Y. Huang, Y. Cheng, *J. Am. Soc. Mass Spectrom.* 22 (2011).
- [144] K.Y. Niu, J. Yang, S.A. Kulnich, J. Sun, H. Li, X.W. Du, *J. Am. Chem. Soc.* 132 (2010) 9814–9819.
- [145] W.T. Nichols, T. Sasaki, N. Koshizaki, *J. Appl. Phys.* 100 (2006), 114911.
- [146] P.V. Kazakevich, A.V. Simakin, V.V. Voronov, G.A. Shafeev, *Appl. Surf. Sci.* 252 (2006) 4373–4380.
- [147] T.X. Phuoc, B.H. Howard, D.V. Martello, Y. Soong, M.K. Chyu, *Opt. Laser Eng.* 46 (2008) 829–834.
- [148] L.P. Wang, Y. Leconte, Z. Feng, C. Wei, Y. Zhao, Q. Ma, W. Xu, S. Bourrioux, P. Azais, M. Srinivasan, Z.J. Xu, *Adv. Mater.* 29 (2017), 1603286.
- [149] Y. Qin, Q. Li, J. Xu, X. Wang, G. Zhao, C. Liu, X. Yan, Y. Long, S. Yan, S. Li, *Electrochim. Acta* 224 (2017) 90–95.
- [150] X. Teng, Y. Qin, X. Wang, H. Li, X. Shang, S. Fan, Q. Li, J. Xu, D. Cao, S. Li, *Nanoscale Res. Lett.* 13 (2018) 60.
- [151] M. Monthieux, V.L. Kuznetsov, *Carbon* 44 (2006) 1621–1623.
- [152] Honghui Chen, Yanfeng Ma, Tengfei Zhang, Bin Qin, *Carbon* (2016).
- [153] F. Du, Y. Ma, X. Lv, Y. Huang, F. Li, Y. Chen, *Carbon* 44 (2006) 1327–1330.
- [154] S. Cui, P. Scharff, C. Siegmund, L. Spiess, H. Romanus, *Carbon* 41 (2003) 1648–1651.
- [155] H. Qiu, Z. Shi, L. Guan, L. You, M. Gao, S. Zhang, J. Qiu, Z. Gu, *Carbon* 44 (2006) 516–521.
- [156] Y.S. Park, K.S. Kim, H.J. Jeong, W.S. Kim, J.M. Moon, K.H. An, D.J. Bae, Y.S. Lee, G.-S. Park, Y.H. Lee, *Synth. Met.* 126 (2002) 245–251.
- [157] Z. Shi, Y. Lian, F.H. Liao, X. Zhou, Z. Gu, Y. Zhang, S. Iijima, H. Li, K.T. Yue, S.-L. Zhang, *J. Phys. Chem. Solids* 61 (2000) 1031–1036.
- [158] E.G. Gamaly, T.W. Ebbesen, *Phys. Rev. B* 52 (1995) 2083.
- [159] W.A. De Heer, P. Poncharal, C. Berger, J. Gezo, Z. Song, J. Bettini, D. Ugarte, *Science* 307 (2005) 907–910.
- [160] O.A. Louchev, Y. Sato, H. Kanda, *Phys. Rev. E* 66 (2002), 011601.

- [161] O.A. Louchev, Y. Sato, H. Kanda, *J. Appl. Phys.* 91 (2002) 10074–10080.
- [162] O.A. Louchev, J.R. Hester, *J. Appl. Phys.* 94 (2003) 2002–2010.
- [163] Y.W. Liu, L. Wang, H. Zhang, *Chem. Phys. Lett.* 427 (2006) 142–146.
- [164] W. Qi, M. Wang, *J. Mater. Sci. Lett.* 21 (2002) 1743–1745.
- [165] A.J. Fetterman, Y. Raitses, M. Keidar, *Carbon* 46 (2008) 1322–1326.
- [166] M. Keidar, I. Levchenko, T. Arbel, M. Alexander, A.M. Waas, K. Ostrikov, *Appl. Phys. Lett.* 92 (2008), 043129.
- [167] M. Suda, Y. Takeda, K. Sujishi, T. Tanaka, *J. Biochem.* 38 (1951) 297–302.
- [168] P. Allia, M. Baricco, P. Tiberto, F. Vinai, *J. Appl. Phys.* 74 (1993) 3137–3143.
- [169] R.S. Averback, H. Hahn, H. Höfler, J. Logas, *Appl. Phys. Lett.* 57 (1990) 1745–1747.
- [170] F. El-Tantawy, *Eur. Polym. J.* 37 (2001) 565–574.
- [171] Y. Yao, Z. Huang, P. Xie, L. Wu, L. Ma, T. Li, Z. Pang, M. Jiao, Z. Liang, J. Gao, Y. He, D.J. Kline, M.R. Zachariah, C. Wang, J. Lu, T. Wu, T. Li, C. Wang, R. Shahbazian-Yassar, L. Hu, *Nat. Nanotechnol.* 14 (2019) 851–857.
- [172] Y. Yao, Z. Huang, P. Xie, S.D. Lacey, R.J. Jacob, H. Xie, F. Chen, A. Nie, T. Pu, M. Rehwoldt, *Science* 359 (2018) 1489–1494.
- [173] P. Xie, Y. Yao, Z. Huang, Z. Liu, J. Zhang, T. Li, G. Wang, R. Shahbazian-Yassar, L. Hu, *C. Wang, Nat. Commun.* 10 (2019) 1–12.
- [174] Y. Chen, Y. Li, Y. Wang, K. Fu, V.A. Danner, J. Dai, S.D. Lacey, Y. Yao, L. Hu, *Nano Lett.* 16 (2016) 5553–5558.
- [175] Y. Qiao, Y. Liu, C. Chen, H. Xie, Y. Yao, S. He, W. Ping, B. Liu, L. Hu, *Adv. Funct. Mater.* 28 (2018), 1805899.
- [176] S. Zeng, B. Lv, J. Qiao, W. Yang, C. Zhu, Y. Zhang, D. Hu, M. Chen, J. Di, Q. Li, *ACS Appl. Nano Mater.* 2 (2019) 7870–7879.
- [177] Y. Shang, B. Shi, S.M. Doshi, T. Chu, G. Qiu, A. Du, Y. Zhao, F. Xu, E. T. Thostenson, K.K. Fu, *ACS Appl. Mater. Interfaces* (2020).
- [178] J.S.C. Francis, R. Raj, *J. Am. Ceram. Soc.* 95 (2012) 138–146.
- [179] Y. Li, W. Han, G. Chen, Y. Cheng, K. Gui, *Mater. Lett.* 174 (2016) 122–125.
- [180] K.A. Khor, K.H. Cheng, L.G. Yu, F. Boey, *Mater. Sci. Eng. A Struct.* 347 (2003) 300–305.
- [181] R. Baraki, S. Schwarz, O. Guillon, *J. Am. Ceram. Soc.* 95 (2012) 75–78.
- [182] T. Jiang, Y. Liu, Z. Wang, W. Sun, J. Qiao, K. Sun, *J. Power Sources* 248 (2014) 70–76.
- [183] R. Muccillo, M. Kleitz, E.N. Muccillo, *J. Eur. Ceram. Soc.* 31 (2011) 1517–1521.
- [184] C. Wang, W. Ping, Q. Bai, H. Cui, R. Hensleigh, R. Wang, A.H. Brozena, Z. Xu, J. Dai, Y. Pei, *Science* 368 (2020) 521–526.
- [185] P. Dong, Z. Wang, W. Wang, S. Chen, J. Zhou, *Scr. Mater.* 123 (2016) 118–121.
- [186] J.S. Lee, O.S. Kwon, S.J. Park, E.Y. Park, S.A. You, H. Yoon, J. Jang, *ACS Nano* 5 (2011) 7992–8001.
- [187] Z. Zeng, W. Zhang, Y. Liu, P. Lu, J. Wei, *Electrochim. Acta* 256 (2017) 232–240.
- [188] Y. Liu, Z. Zeng, J. Wei, *Front. Nanosci. Nanotechnol.* 2 (2016) 78.
- [189] Y. Liu, Z. Zeng, B.P. Bloom, D.H. Waldeck, J. Wei, *Small* 14 (2018), 1703237.
- [190] Y. Yao, Z. Huang, P. Xie, S.D. Lacey, R.J. Jacob, H. Xie, F. Chen, A. Nie, T. Pu, M. Rehwoldt, D. Yu, M.R. Zachariah, C. Wang, R. Shahbazian-Yassar, J. Li, L. Hu, *Science* 359 (2018) 1489–1494.
- [191] C. Yang, M. Cui, N. Li, Z. Liu, S. Hwang, H. Xie, X. Wang, Y. Kuang, M. Jiao, D. Su, L. Hu, *Nano Energy* 63 (2019), 103855.
- [192] Y. Liu, P. Li, F. Wang, W. Fang, Z. Xu, W. Gao, C. Gao, *Carbon* 155 (2019) 462–468.
- [193] J. Sun, W. Wang, Q. Yue, *Materials* 9 (2016) 231.
- [194] Z. Liu, J. Wang, V. Kushvaha, S. Poyraz, H. Tippur, S. Park, M. Kim, Y. Liu, J. Bar, H. Chen, X. Zhang, *Chem. Commun.* 47 (2011) 9912–9914.
- [195] L.C. Qin, D. Zhou, A.R. Krauss, D.M. Gruen, *Appl. Phys. Lett.* 72 (1998) 3437–3439.
- [196] C. Bower, O. Zhou, W. Zhu, D.J. Werder, S. Jin, *Appl. Phys. Lett.* 77 (2000) 2767–2769.
- [197] X. Zhou, L. Shen, L. Li, S. Zhou, T. Huang, C. Hu, W. Pan, X. Jing, J. Sun, L. Gao, Q. Huang, *J. Eur. Ceram. Soc.* 33 (2013) 2119–2126.
- [198] T. Lin, Z. Liu, M. Zhou, H. Bi, K. Zhang, F. Huang, D. Wan, Y. Zhong, *ACS Appl. Mater. Interfaces* 6 (2014) 3088–3092.
- [199] H.-C. Su, C.-H. Chen, Y.-C. Chen, D.-J. Yao, H. Chen, Y.-C. Chang, T.-R. Yew, *Carbon* 48 (2010) 805–812.
- [200] R. Xie, J. Wang, Y. Yang, K. Jiang, Q. Li, S. Fan, *Compos. Sci. Technol.* 72 (2011) 85–90.
- [201] M.N. Nadagouda, R.S. Varma, *Macromol. Rapid Commun.* 28 (2007) 842–847.
- [202] D. Voiry, J. Yang, J. Kupferberg, R. Fullon, C. Lee, H.Y. Jeong, H.S. Shin, M. Chhowalla, *Science* 353 (2016) 1413–1416.
- [203] S. Xu, G. Zhong, C. Chen, M. Zhou, D.J. Kline, R.J. Jacob, H. Xie, S. He, Z. Huang, J. Dai, *Matter* 1 (2019) 759–769.
- [204] Y. Kang, W. Li, T. Ma, X. Huang, Y. Mo, Z. Chu, Z. Zhang, G. Feng, *Compos. Sci. Technol.* 174 (2019) 184–193.
- [205] T. Zhu, S. Li, B. Ren, L. Zhang, L. Dong, L. Tan, *J. Mater. Sci.* 54 (2019) 9632–9642.
- [206] K.H. Lee, J. Oh, J.G. Son, H. Kim, S.-S. Lee, *ACS Appl. Mater. Interfaces* 6 (2014) 6361–6368.
- [207] K.Y. Foo, B.H. Hameed, *Bioresour. Technol.* 119 (2012) 234–240.
- [208] H. Lv, Y. Guo, Z. Yang, Y. Cheng, L.P. Wang, B. Zhang, Y. Zhao, Z.J. Xu, G. Ji, *J. Mater. Chem. C* 5 (2017) 491–512.
- [209] P.C.P. Watts, W.-K. Hsu, A. Barnes, B. Chambers, *Adv. Mater.* 15 (2003) 600–603.
- [210] Y. Zhu, S. Murali, M.D. Stoller, K.J. Ganesh, W. Cai, P.J. Ferreira, A. Pirkle, R. M. Wallace, K.A. Cychoz, M. Thommes, D. Su, E.A. Stach, R.S. Ruoff, *Science* 332 (2011) 1537–1541.
- [211] H. Hu, Z. Zhao, Q. Zhou, Y. Gogotsi, J. Qiu, *Carbon* 50 (2012) 3267–3273.
- [212] Y. Du, T. Liu, B. Yu, H. Gao, P. Xu, J. Wang, X. Wang, X. Han, *Mater. Chem. Phys.* 135 (2012) 884–891.
- [213] Q. Liu, J. Gu, W. Zhang, Y. Miyamoto, Z. Chen, D. Zhang, *J. Mater. Chem.* 22 (2012) 21183–21188.
- [214] J.M. Kim, D. Ko, J. Oh, J. Lee, T. Hwang, Y. Jeon, W. Hooch Antink, Y. Piao, *Nanoscale* 9 (2017) 15582–15590.
- [215] X. Chen, X. Bo, W. Ren, S. Chen, C. Zhao, *Mater. Chem. Front.* 3 (2019) 1433–1439.
- [216] M. Zong, Y. Huang, Y. Zhao, X. Sun, C. Qu, D. Luo, J. Zheng, *RSC Adv.* 3 (2013) 23638–23648.
- [217] R. Kumar, S.M. Yousry, K.Z. Ya, W.K. Tan, G. Kawamura, A. Matsuda, *Diam. Relat. Mater.* 101 (2020), 107622.
- [218] M. Yang, K.G. Lee, S.J. Lee, S.B. Lee, Y.-K. Han, B.G. Choi, *ACS Appl. Mater. Interfaces* 7 (2015) 22364–22371.
- [219] R. Kumar, R.K. Singh, A.K. Singh, A.R. Vaz, C.S. Rout, S.A. Moshkalev, *Appl. Surf. Sci.* 416 (2017) 259–265.
- [220] G. Zhong, S. Xu, C. Chen, D.J. Kline, M. Giroux, Y. Pei, M. Jiao, D. Liu, R. Mi, H. Xie, B. Yang, C. Wang, M.R. Zachariah, L. Hu, *Adv. Funct. Mater.* 29 (2019), 1904282.
- [221] G. Li, T. Xie, S. Yang, J. Jin, J. Jiang, *J. Phys. Chem. C* 116 (2012) 9196–9201.
- [222] Y. Fan, H. Yang, M. Li, G. Zou, *Mater. Chem. Phys.* 115 (2009) 696–698.
- [223] A.N. Yusoff, M.H. Abdullah, S.H. Ahmad, S.F. Jusoh, A.A. Mansor, S.A.A. Hamid, *J. Appl. Phys.* 92 (2002) 876–882.
- [224] Y. Zhang, Y. Huang, T. Zhang, H. Chang, P. Xiao, H. Chen, Z. Huang, Y. Chen, *Adv. Mater.* 27 (2015) 2049–2053.
- [225] Z. Chen, C. Xu, C. Ma, W. Ren, H.-M. Cheng, *Adv. Mater.* 25 (2013) 1296–1300.
- [226] N. Yousefi, X. Sun, X. Lin, X. Shen, J. Jia, B. Zhang, B. Tang, M. Chan, J.-K. Kim, *Adv. Mater.* 26 (2014) 5480–5487.
- [227] H. Fei, J. Dong, C. Wan, Z. Zhao, X. Xu, Z. Lin, Y. Wang, H. Liu, K. Zang, J. Luo, *Adv. Mater.* 30 (2018), 1802146.
- [228] Y. Liu, Z. Ge, Z. Sun, Y. Zhang, C. Dong, M. Zhang, Z. Li, Y. Chen, *Nano Energy* 67 (2020), 104216.
- [229] H. Yoshida, T. Sugai, H. Shinohara, *J. Phys. Chem. C* 112 (2008) 19908–19915.



Yiyang Liu got his master's degree from the Physics department of Arizona State University in 2013, with Prof. Michael O'Connell as the advisor. In University of North Carolina at Greensboro, he accomplished the Ph.D. work in 2017. Currently, he joined Zhengzhou University to extend his research on carbon-based nanomaterials and their applications.



Zhen Ge graduated from Nankai University with a Ph.D. degree in materials physics and chemistry in 2019 and then joined Nankai University for his postdoctoral studies. His research interests mainly focus on graphene composites, porous materials and energy storage.



Zhongjun Li is a Professor of the College of Chemistry in Zhengzhou University. He received his Ph.D. from Central South University. His research interests include: 1. Design and synthesis of Photocatalysts for CO₂ Reduction; 2. Design and synthesis of photocatalysts for hydrogen production from water under light; 3. Lithium-air batteries\lithium sulfur batteries and other electrochemical energy storage\conversion materials.



Prof. Yongsheng Chen graduated from the University of Victoria with a Ph.D. degree in chemistry in 1997 and then joined the University of Kentucky and the University of California at Los Angeles for postdoctoral studies from 1997 to 1999. From 2003, he has been a Chair Professor at Nankai University. His main research interests include: i) carbon-based nanomaterials, including carbon nanotubes and graphene; ii) organic and polymeric functional materials, and iii) energy devices including organic photovoltaics and supercapacitors.